THE EFFECT OF PERLITE AND MINERAL WOOL LEACHATE SOLUTIONS ON THE CORROSION BEHAVIOURS OF PIPELINE STEELS

by

Gerard Chlela

Submitted in partial fulfilment of the requirements
for the degree of Master of Applied Sciences

at

Dalhousie University
Halifax, Nova Scotia
August 2023

Dalhousie University is located in Mi'kma'ki, the
ancestral and unceded territory of the Mi'kmaq.
We are all Treaty people.

TABLE OF CONTENTS:

LIST OF TABLES

LIST OF FIGURES

Abstract

This study provides an extensive in-depth analysis of the issue of corrosion under insulation (CUI), with an overview of the capabilities and limitations of the latest nondestructive evaluation techniques, commonly employed for inspection of CUI systems. CUI is difficult to identify because it remains hidden beneath the insulation hardware, often resulting in unexpected failures, and can occur under any class of insulating material. The main problem to address is the ingress of water into the insulation, through damaged sealants and compounds to form leachate solutions. Given the paramount significance of insulation choice in influencing Corrosion Under Insulation (CUI), the study focused on investigating two distinct insulation types: perlite and mineral wool insulation. Leachate solutions were meticulously extracted from these insulations, forming the basis for subsequent comprehensive testing procedures. These solutions were used in the experimental phase where (12) AISI 1018 steel coupons and (12) X52 coupons were examined. A diverse array of tests was employed to discern the composition of the solutions, delve into the surface properties of the tested coupons, and quantify corrosion rates. Through this systematic approach, our objective was to uncover the profound impact of insulation on corrosion dynamics and to elucidate how the selection of insulation for a given pipeline system can significantly influence the system's lifespan, either by mitigating or expediting the corrosion process.

Keywords:

Corrosion, corrosion under insulation, mineral wool insulation, perlite insulation, leachate solution.

LIST OF ABREVIATIONS USED

CUI	Corrosion Under Insulation
ICP	Inductively Coupled Plasma
EDS	Energy-dispersive X-ray spectroscopy
SEM	Scanning Electron Microscopy
EIS	Electrochemical Impedance Spectroscopy
PD	Potentiodynamic
MLCR	Mass Loss Corrosion Rate
LSP	Linear Sweep Polarization
Err	Error
P – 45 – 20	Perlite leachate solution, aged for 45 days, with 20 g of insulation
MW – 0 – 20	Mineral Wool solution, aged for 0 days, with 20 g of insulation
HCO_3^-	Bicarbonate ions
CO_3^{2-}	Carbonate ions
OH^-	Hydroxide ions
CR	Corrosion Rate
E_{corr}	E corrosion (corrosion potential)
I_{corr}	I corrosion (corrosion current)
R_p	Polarization Resistance

Chapter 1: Introduction

Corrosion under insulation (CUI) is a significant issue encountered by industries utilizing insulation systems. It stands as a persistent and costly challenge in industries where pipes, vessels, and equipment are subjected to the relentless onslaught of harsh environmental conditions. CUI is not a new problem, but can it surely be defined as a serious one.

Leachate solutions are generated when insulation materials encounter moisture or when insulation systems are improperly designed or installed. Moisture sources can include external factors like rainwater or steam leaks and internal sources such as condensation within the insulation system. When moisture permeates the insulation, it can react with chemical components of the insulation material, releasing corrosive substances. The nature of these leachates, whether acidic or alkaline, depends on the insulation material and environmental conditions. Leachates could increase the conductivity of moisture, accelerating the corrosion rate and promoting the formation of localized corrosion cells. Within this complex realm, the choice of insulation emerges as a paramount determinant, wielding a profound impact on the overall performance and longevity of the systems. The importance of selecting the appropriate insulation type cannot be overstated, as it plays a pivotal role in either safeguarding against or exacerbating the corrosive forces that lurk beneath.

At its core, the primary function of insulation is to control temperature gradients, thereby preventing energy loss and facilitating the efficient operation of industrial equipment. However, this seemingly innocuous layer of protection can inadvertently provide a haven for the insidious duo of moisture and contaminants. When moisture infiltrates the insulation layer, it creates a microenvironment that fosters corrosion. This is the genesis of the CUI phenomenon, where corrosion takes root unbeknownst to external observation, steadily gnawing away at the integrity of the underlying substrate.

The diverse array of insulation materials available in the market introduces a complex matrix of possibilities, each with its own inherent properties and susceptibility to facilitating or impeding CUI. The intrinsic porosity, permeability, and water absorption characteristics of these materials influence their propensity to trap moisture, with some materials serving as better barriers than others. Consider, for instance, the selection of an insulation material with high water repellency as a strategic defense against CUI. The

intricate interplay between insulation properties, environmental conditions, and corrosion dynamics underscores the nuanced nature of the challenge at hand. The economic ramifications of CUI-related failures reverberate far beyond the immediate costs of repairing or replacing corroded equipment. Downtime resulting from unexpected maintenance, reduced operational efficiency, environmental hazards, and safety risks collectively underline the gravity of the issue. Choosing the right insulation type, therefore, becomes an investment in long-term operational reliability and cost-effectiveness. In essence, the significance of insulation selection in the CUI process encapsulates a complete perspective that involves material science, engineering practices, and operational considerations. The interaction between corrosion specialists, materials scientists, engineers, and industry stakeholders is crucial in navigating the complicated landscape of CUI prevention. Industries must recognize that the choice of insulation is not a mere technicality, but a strategic decision that can tip the scales between optimal system performance and the gradual erosion of equipment integrity. As industries evolve and technology advances, the imperative to make informed insulation choices gains even more prominence. With a comprehensive understanding of insulation's role in either enabling or thwarting corrosion, industries can pave the way for a future where systems remain resilient, efficient, and corrosion-free for their intended lifespans.

1.1 Thesis objectives:

The objectives of this study are to explore:

- The phenomenon of corrosion under insulation and the factors promoting this phenomenon
- Study the corrosion under perlite and mineral wool insulation due to leachate solutions
- Impact of leachate solutions on X52 steel and AISI 1018 steel
- Significance of insulation selection on the corrosion process

1.2 Thesis structure:

The following section provides an overview of the structural framework that governs the organization and presentation of this thesis.

After the introduction, the thesis is divided into four chapters:

- Background and literature review
- Experimental procedures
- Results and discussions
- Conclusions

Chapter 2: Background

This chapter navigates through a detailed exploration of corrosion and its various types, unveiling their underlying processes and effects.

2.1 Principle of corrosion

The term corrosion has been described since ancient times. It is most commonly known as rust, an undesirable occurrence due to its ability to destroy the allure and shine of objects, while in turn shortening their lifespan. The impact of corrosion on daily human lives and progression has been noted throughout history. Corrosion, though naturally occurring, is a costly destructive phenomenon comparable to natural disasters such as earthquakes, volcanoes, etc. [1].

The formation of a corrosion cell allows for corrosion to take place. A corrosion cell, shown in Figure 1, consists of four components:

1. Anode (oxidation)
2. Cathode (reduction)
3. Electrolyte (ionic path)
4. Metallic path (electron path)

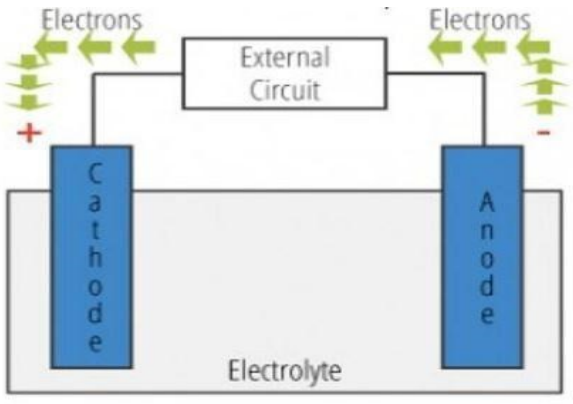

Figure 1 - Corrosion cell [2]

For a better understanding of the corrosion mechanisms, Pourbaix diagrams offer a foundational grasp of the thermodynamics behind these processes. This comprehension is fundamental in devising strategies to prevent and control corrosion effectively, while also

enabling accurate predictions of the potential corrosion products that might manifest on metals or alloys within distinct environmental conditions. Figure 2 shows the Pourbaix diagram corresponding to iron.

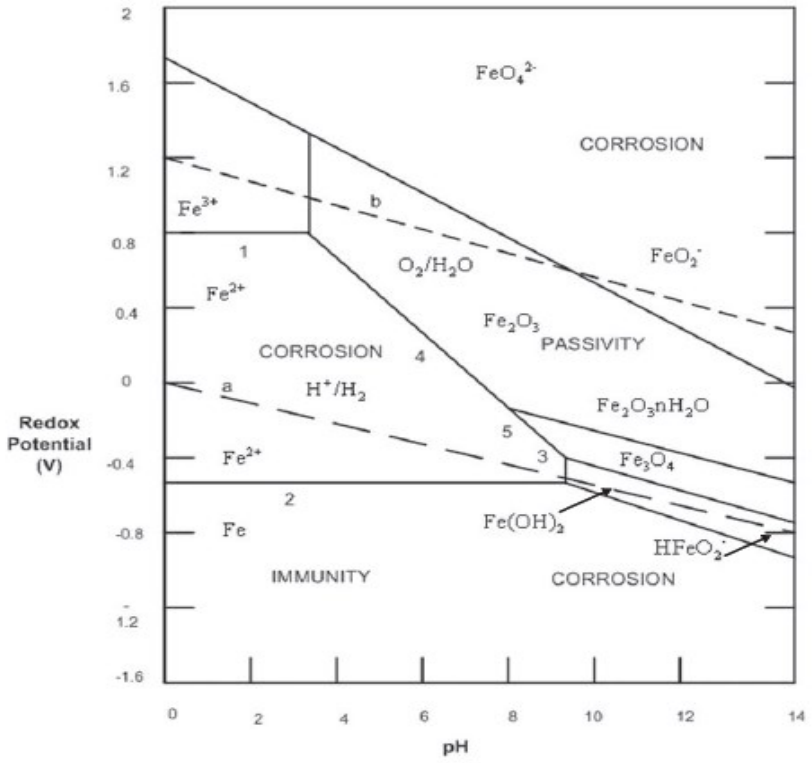

Figure 2 - Pourbaix diagram for iron [3]

2.2 Types of corrosion

2.2.1 Uniform corrosion

Uniform corrosion occurs with the uniform thinning of a metal, without any specific pin-pointed cause, and does not commonly affect the substrate from deep within. A frequently occurring and common example is when steel rusts in open air (Figure 3). This results in a corrosion attack that creates a substantial loss of the metal weight. This most commonly occurs when steel structures are unused and left to rust. A uniform attack is generally easy to detect and has a predictable outcome. Therefore, it is less detrimental than the other types of corrosion [4].

Figure 3 - Uniform corrosion [5]

2.2.2 Galvanic corrosion

Galvanic corrosion occurs when two dissimilar metals are in contact with one another in a corrosive electrolyte, setting up a galvanic cell, where a chemical change occurs and becomes an energy source [6]. Table 1 presents a comprehensive galvanic corrosion chart, illustrating the behavior of various metals in different galvanic pairings.

Table 1 - Galvanic corrosion chart.

Magnesium **Anodic (least noble) corroded**
Magnesium alloys
Zinc
Beryllium
Aluminum 110, 3003, 3004, 5052, 6053
Cadmium
Aluminum 2017, 2024, 2117
Mild steel 1018, wrought iron
HSLA steel, cast iron
Chrome iron (active)
430 Stainless (active)
302, 303, 321, 347, 410, 416 Stainless steel (active)
Ni-resist
316, 317 Stainless (active)
Carpenter 20Cb-3 stainless (active)
Aluminum bronze (CA687)
Hastelloy C (active) Inconel 625 (active titanium (active))
Lead/tin solder
Lead
Tin
Inconel 600 (active)
Nickel (active)
60% Ni–15% Cr (active)

80% Ni–20% Cr (active)
Hastelloy B (active)
Naval brass (CA464), yellow brass (CA268)
Red brass (CA230), admiralty brass (CA443)
Copper (CA102)
Manganese bronze (CA675), Tin bronze (CA903, 905)
410, 416 Stainless (passive) phosphor bronze (CA521, 524)
Silicon bronze (CA651, 655)
Nickel silver (CA732, 735, 745, 752, 754, 757, 765, 770, 794)
Cupro nickel 90–10
Cupro nickel 80–20
430 Stainless (passive)
Cupro nickel 70–30
Nickel aluminum bronze (CA630, 632)
Monel 400, K500
Silver solder
Nickel (passive)
60% Ni–15% Cr (passive)
302, 303, 304, 321, 347 Stainless (passive)
316, 317 Stainless (passive)
Carpenter 20Cb–3 Stainless (passive), Incoloy 825 (passive)
Silver
Titanium (passive), Hastelloy C and C276 (passive)
Graphite
Ziconium
Gold
Platinum **Cathodic (most noble) protected**

2.2.3 De-alloying

De-alloying and selective leaching refer to the process of corroding of one or more components of a solid solution alloy. A specific type of de-alloying is dezincification, where zinc is targeted in zinc containing alloys, such as brasses [7].

2.2.4 Crevice corrosion

Crevice corrosion is often triggered by localized corrosion caused by the accumulation of dirt, dust, mud, and other materials on the metal surface. Additionally, it can occur in the presence of voids, gaps, or cavities along interconnected surfaces. The crucial factor enabling this type of corrosion is the formation of a differential aeration cell, shown in Figure 4 [6].

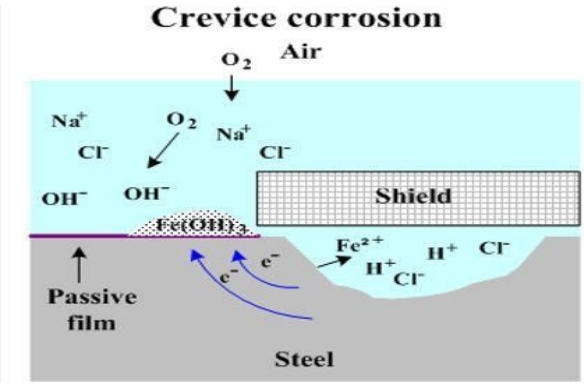

Figure 4 - Crevice corrosion [8]

2.2.5 Pitting corrosion

Pitting corrosion is a localized form of corrosion that takes place on the surface of a metal, where small areas corrode in a preferential manner. This type of corrosion leads to the formation of cavities or pits, though most of the surface remains whole. Metals like aluminum and stainless-steel form passive films and are therefore more susceptible to this kind of corrosion. It is the most destructive form of corrosion and can cause failure by penetrating with only a minor percent of weight-loss of the total structure. It is a prominent kind of failure found in the chemical processing industry. The entire system requires replacement due to the destructive nature of pitting corrosion [1].

2.2.6 Intergranular corrosion

Intergranular corrosion is a localized form of corrosion where a tapered path is oxidized along a metal's grain boundaries, where a tapered path is oxidized preferentially along a metal's grain boundaries (Figure 5) [1].

Figure 5 - Localized attack of intergranular corrosion [9]

2.2.7 Stress corrosion cracking (SCC)

SCC is the sudden and unpredictable failure of a metal due to the dual action of static stress and exposure to a specific environment. In many instances, the cause can also be traced back to a metallurgical condition, leading to the initiation and propagation of a notable crack. The failures that occur usually cannot be predicted. They can take place after as little as a few months or years of service [1].

2.2.8 Hydrogen damage

Hydrogen damage occurs when atomic hydrogen diffuses back into the metal, resulting in either blistering if it forms molecular hydrogen in internal voids or embrittlement if it permeates in the lattices. In the natural corrosion processes, the formation of atomic hydrogen can occur as a cathodic reaction (Figure 6) [4].

Figure 6 - Hydrogen blistering [10]

2.2.9 Corrosion under insulation (CUI)

CUI generally occurs on low-carbon alloy steel , and austenitic stainless-steels surrounded by thermal insulation e.g. piping systems, pressure vessels, and tanks (Figure 7) [11]. CUI occurs when water or contaminants penetrate the insulation or fireproofing materials. The water ingress is mostly through damaged weather jacketing systems and weather barriers, resulting in the creation of annular space between the insulation and the pipe surface, where these agents can be held for a long duration of time. As a result, corrosion begins on the insulated surface of metal and an unpredicted and spontaneous failure could take place [12]. In addition, the materials used for insulation, such as calcium silicate and polyurethane foams, have varying amounts of fluoride, chloride, bromide, and sodium ions. When moisture penetrates these insulations, these ions are leached from the material, causing an increase in the rate of corrosion under insulation systems as solutions with low pH may form [13].

Figure 7 - corrosion under insulation process [14]

Factors promoting corrosion under insulation:

The most important factor in avoiding CUI is to prevent water from touching the surface of the metal Figure 8. The risk of corrosion is impacted by insulation materials, as they have a capacity for absorption. The wetting of insulation on equipment encourages the conditions of corrosion to initiate Figure 8 [15].

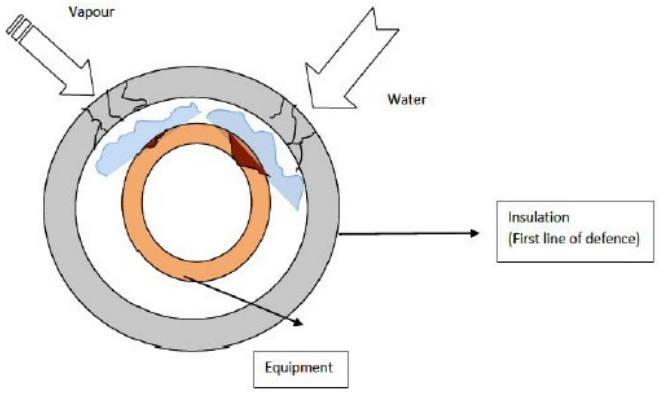

Figure 8 - CUI mechanism [16]

Insulation and jacketing materials:

An effective strategy for designers of industrial equipment and piping involves three key measures (Figure 9):

1) High-quality coatings.

2) Implementing a weather barrier jacketing system.

3) Making informed choices regarding the insulation material [17].

All types of insulation allow for CUI of carbon steel underneath, though the rate of corrosion may vary depending on the type of insulation material. Factors such as the presence of water-leachable salt , residual compounds, water retention, permeability, and wettability greatly influence the rate of CUI [18]. Thus, materials selection plays a crucial role in reducing CUI.

Jacketing serves as a barrier to shield the underlying material from external elements, mechanical damage, or other potential hazards. Good jacketing materials are those that possess a combination of properties suitable for the intended application, ensuring effective protection and long-lasting performance. The selection of the appropriate jacketing material depends on factors such as the application environment, the material being protected, cost considerations, and specific performance requirements. For instance: polyvinyl chloride (PVC), polyethylene (PE), polypropylene (PP), aluminum (Al), and other materials are commonly used as jacketing materials [19].

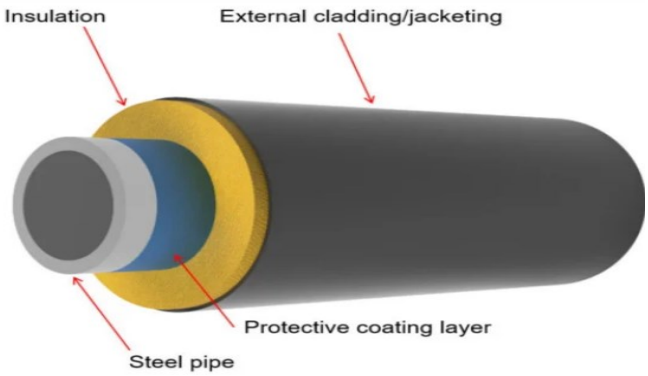

Figure 9 - A typical insulated pipe schematic, which includes an exterior cladding/jacketing, insulating material, a protective coating layer, and the steel pipe itself [11]

The choice of materials for pipes:

The choice of materials for pipes can affect the corrosion under insulation (CUI) process. Certain materials are more prone to CUI than others. For example, carbon steel pipes are particularly susceptible to CUI due to their low resistance to corrosion. On the other hand, materials such as stainless steel and corrosion-resistant alloys are less susceptible to CUI. Carbon steel under wet insulation displays nonuniform general corrosion and/or highly localized pitting. Austenitic stainless steels pit and experience chloride stress corrosion cracking CSCC [18]. Factors such as the pipe material's composition, surface condition, and protective coatings can influence the severity and rate of CUI.

Environmental condition:

CUI is significantly affected by chloride ions and other contaminants in the environment. When insulated equipment, especially those operating at high temperatures, is exposed to such an environment, water laden with these dissolved contaminants can penetrate the insulation, reaching the surface of the equipment. Subsequently, as this water evaporates it leaves behind these contaminants as salts. [13]. There will be an increase of salt concentration as more water penetration and evaporation cycles take place. As such, low chloride concentrations in the air or in sea water can quicken the corrosion rate on the insulated equipment. Besides chlorides, marine environments often contain other corrosive elements, such as sulfur compounds or industrial pollutants. These contaminants, when combined with moisture in the atmosphere, convert to sulfuric and sulfurous acid,

producing acid rain. Acid water (and oxygen) can penetrate insulation and as a result, trigger the acceleration of corrosion on the surface of metals [20].

pH Effect:

Acidic conditions under insulation can cause serious corrosion problems. Water with pH values of 6 or below can lead to general and pitting corrosion of carbon steel pipes. Combined with temperatures above 60°C may lead to SCC of stainless steel pipes [21]. Figure 10 displays the impact of pH levels on the rate of corrosion of iron in aerated water at room temperature. As can be seen, the rate of corrosion considerably increases as the level of pH drops under 6. In wet insulation, the rate of corrosion can rise to 20 times more than the corrosion of bare metals that have been exposed to atmospheric conditions. Some sealants, caulking compounds, and insulation materials produce acidic solutions when wet because of water leachable components [22].

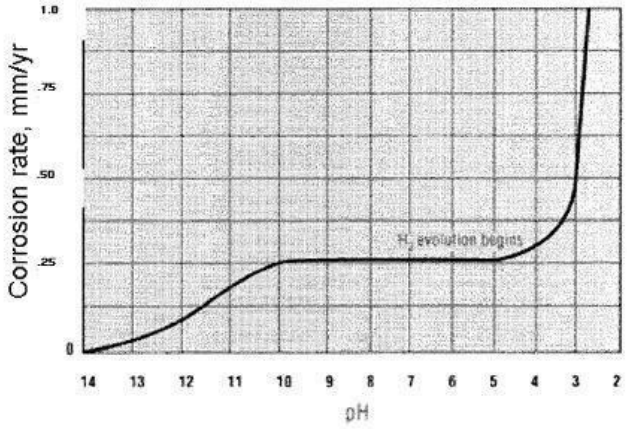

Figure 10 - Effect of pH on corrosion at room temperature in aerated water [13]

Moisture

Atmospheric conditions in the location where insulation systems are being used are crucial factors that must be taken into consideration to evaluate their natural influence on CUI. For atmospheric corrosion to take place in areas that do not have air pollution, a relative humidity of 80% is needed. Iron corrosion happens at a relative humidity of around 50% in polluted areas. In addition to that, temperature fluctuations cycles of heating and cooling,

especially rapid changes, can lead to expansion and contraction of insulation systems. This can cause cracking, gaps, or the insulation damage, allowing moisture ingress [23].

Service temperature

The potential development of CUI can be influenced by various factors such as the operating temperature within the process where the insulated equipment is [24]. CUI exhibits heightened aggressiveness in situations where operating temperatures result in frequent condensation and subsequent evaporation of atmospheric moisture [17]. Therefore, a crucial factor that triggers corrosion under insulation is service temperature. It has been proven that carbon steel equipment that functions at temperatures registered between -4°C and 150°C is greatly at risk of being affected by corrosion. Figure 11 shows the impact of temperature on steel corrosion in an open system in water, in a closed system, and under thermal insulation [20].

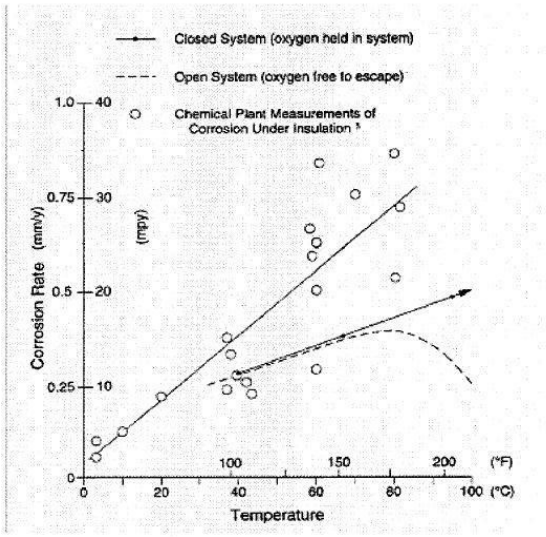

Figure 11- Influence of temperature on the corrosion of carbon steel in water [25]

Mechanical design of equipment and insulation installation

The geometry of equipment and relevant attachments greatly impacts corrosion under insulation. Overall, irregularly configured equipment with many attachments like support rings, brackets, pressure and temperature gauge devices, etc. are at a higher risk of

corrosion and its resulting issues. An insulation system that has been poorly installed is a pivotal factor in the resulting performance of the system. It can promote corrosion on the underlying steel surface[26].

Mechanical damage

Since corrosion cannot take place in the absence of water, mechanical damage to an insulation system (particularly caulking compounds and weather barriers) can ease the seepage of water right into the system. A frequent example of mechanical abuse is people walking atop insulated pipe systems or climbing into vessels to perform routine maintenance. If the aluminum jacketing were deformed for example by impacts, scratches, bending… This would allow water to penetrate the system whenever it rains. As a result, CUI takes place on the surface of the vessel and causes expensive repairs and new insulation to be set up.

2.3 Leachate solutions

Among the various factors influencing CUI, the presence of leachate solutions can intensify the corrosion process. Leachate solutions are formed when water or other chemicals leach out from the insulation material and interact with the metal surface [27]. In this study, the detrimental effects of leachate solutions on corrosion under insulation will be examined, specifically investigating the consequences of this issue in relation to perlite and mineral wool insulation.

Leachate solutions can form through a process known as leaching. They are typically formed when insulation materials come into contact with moisture. Over time, these materials can absorb water, from the environment or the process fluid within the insulated system, which in turn leaches soluble components from the solid material forming a corrosive solution capable of accelerating the corrosion process. This process can be influenced by several factors, including temperature, moisture levels, and the nature of the solid material [28].

These leachate solutions often act as electrolytes, promoting the electrochemical reactions responsible for corrosion as they provide a conductive medium, facilitating the flow of ions necessary for corrosion cells to develop. This enhances the corrosion rate and can lead to

localized or generalized metal loss. Leachate solutions may have varying pH levels, ranging from acidic to alkaline, depending on the insulation material and absorbed substances. Significant pH deviations from the metal's corrosion resistance range can lead to accelerated corrosion rates, whereby acidic solutions tend to cause localized corrosion, while alkaline solutions may induce general corrosion [29]. Certain chemicals present in leachate solutions can have a direct corrosive effect on metals. For example, chlorides and sulfates commonly found in industrial environments can initiate pitting or stress corrosion cracking (SCC) when in contact with susceptible alloys. Leachate solutions that contain corrosive chemicals can significantly exacerbate CUI [30]. Choosing insulation materials with low water absorption and leaching characteristics can minimize the potential for leachate solution formation. Understanding the compatibility between the insulation material and the process environment is crucial in preventing leachate-related CUI. Therefore, the presence of electrolytes, pH changes, and chemical reactivity within these solutions can accelerate corrosion rates, leading to significant damage to equipment and piping systems. Employing preventive measures such as proper insulation selection, protective coatings, vapor barriers, and regular inspection and maintenance can help mitigate the impact of leachate solutions and minimize the occurrence of CUI.

Chapter 3: Experimental procedures

In the upcoming chapter the materials used, the sample preparation procedures and the various tests used to study corrosion will be explored. These tests will include electrochemical analyses and close examinations of surface properties.

3.1 Materials

The materials used in this study consisted of X52 and AISI 1018 steel coupons as well as two types of insulations, mineral wool, and perlite. All materials were bought from commercial sources and are identical to the ones used by industry in the field.

3.1.1 Steel used

API X52 and AISI 1018 steels were chosen as test material to evaluate the corrosion process in various leachate solutions. API X52 steel is characterized by a microstructure comprising fine perlite and ferrite and is commonly used in the construction of oil and gas pipelines for the transportation of natural gas, crude oil, and other hydrocarbons [31].
Table 2 and Table 3 provide information regarding the chemical makeup of these steels [32].

Table 2 - Composition of the API X52 pipeline steel in terms of its chemical makeup (Wt. %)

C	Mn	Si	P	S	Cu	Ni	Cr	Nb	V	Ti	Al	Fe
0.08	1.05	0.26	0.019	0.003	0.019	0.02	0.02	0.041	0.054	0.002	0.038	Bal.

Table 3 - Composition of the AISI 1018 carbon steell (Wt.%)

Elements	Fe	C	Mn	P	S	Cr	W	Ni	Co
Substrate	98.81 to 99.26	0.18	0.6 to 0.9	0.04 max	0.05 max	0.00	0.00	0.00	0.00

API X52 steel was employed to assess corrosion in accordance with ASTM G31/G189 standards, while AISI 1018 was utilized to appraise corrosion following the guidelines of ASTM C1617.

3.1.2 Insulation

Two types of insulations materials were used perlite and mineral wool.

Perlite insulation is made from naturally occurring volcanic glass (Figure 12). It possesses various desirable characteristics, such as low bulk density, thermal conductivity, sound transmission, and high heat resistance, surface area, and chemical inertness [33], [34], [35], [36].

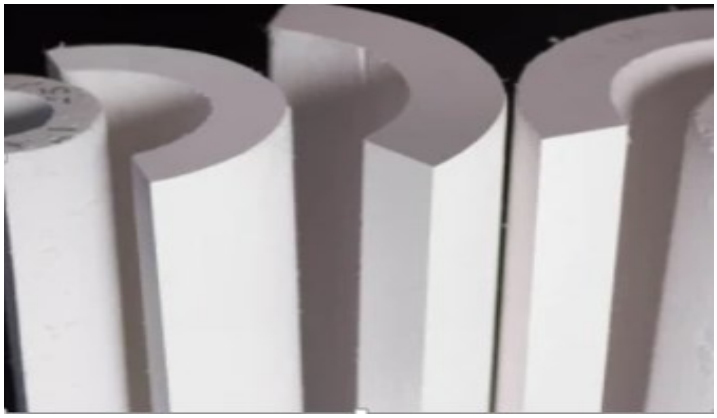

Figure 12 - Perlite insulation

The second insulation type is mineral wool insulation. Mineral wool insulation is made from natural minerals like basalt, diabase, and slag. These minerals are heated to high temperatures, spun into fine fibers, and then formed into sheets or blankets. A small amount of binder may be added to help the fibers stick together. It is classified into glass, stone, and slag wool, and is a widely used thermal insulation material Figure 13. Mineral wool's characteristics include fire-resistant property, acoustic insulation, resists moisture, and provides mechanical strength [37], [38].

Figure 13 - Mineral wool insulation

3.2 Sample preparation

3.2.1 Metal samples

For the autoclave experiments Disks of API X52 were cut from a 1.6 cm diameter bar. The samples were systematically ground using 240, 360, and 600 grit papers, then polished with polycrystalline diamond suspension 9, 3 and 1 microns respectively, then washed with distilled water, and subsequently air-dried at room temperature. For the experiments adhering to the ASTM C1617 standard, AISI 1018 carbon steel rectangular samples measuring (9x7.5) cm were cut from a shim stock sheet.

3.2.2 Artificially aging insulation

Artificially aging insulation is a common practice in the field of insulation testing and research. The purpose of artificially aging insulation is to simulate the effects of natural aging over an extended period within a relatively short timeframe. This accelerated aging process allows researchers and manufacturers to evaluate insulation materials' long-term performance and durability. To artificially age insulation, various methods can be employed, including exposure to elevated temperatures, exposure to specific chemicals, cycling between extreme temperature conditions, or subjecting the insulation to mechanical stress. The specific aging conditions and duration will depend on the purpose of the test and the requirements of the relevant standards or specifications [39].

In order to replicate the deterioration observed during actual usage, the insulation samples were divided into two groups for each type. Both groups underwent artificial aging in an

oven at 150°C for approximately 45 and 90 days respectively (Figure 14). This accelerated aging process was to simulate a phenomenon known as binder burnout, which occurred when insulation is in contact with the "hot" surface of the pipeline. Over time, the insulation adjacent to the pipe surface darkens due to the decomposition of organic binders [40].

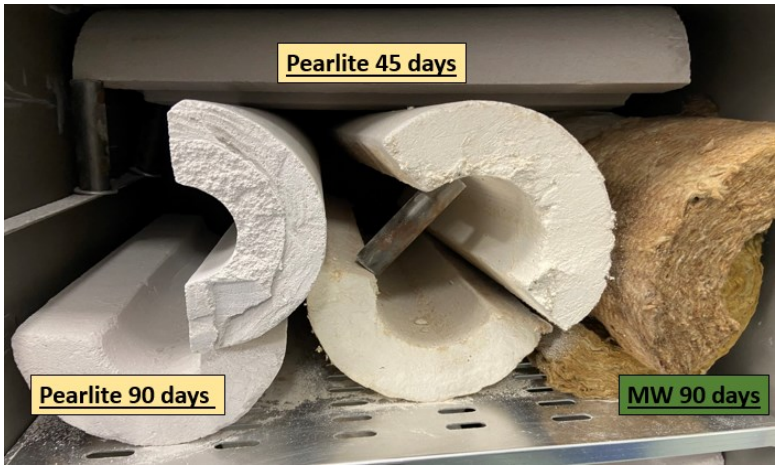

Figure 14 - The insulation will be placed in a furnace to undergo artificial aging for durations of 45 and 90 days.

3.2.3 Leachate solution preparation

Preparing leachate solutions was done according to ASTM C871, where 20 or 80 g of the material to be leached was mixed for 30 s in 400 ml of DI water. The mixture was then transferred to a beaker and brought to a boil for 30 min. After which the mixture was cooled to room temperature and DI water was added to bring its volume to 500 ml. The mixture was then vacuum filtered [41].

In this study, three distinct categories of insulation were used, each corresponding to a specific duration of burning in the furnace: new insulation (0 days aged), insulation aged for 45 days in the furnace, and insulation aged for 90 days. Within each category, two samples were prepared. One with 20g and the other with 80g insulation as shown in Table 4.

Table 4 - The leachate solutions utilized in this study

Type of leachate solutions	Mineral Wool	Perlite
0 days	20 g	20 g
	80 g	80 g
45days	20 g	20 g
	80 g	80 g
90 days	20 g	20 g
	80 g	80 g

3.3 Testing

3.3.1 Inductively Coupled Plasma (ICP)

ICP testing, also known as ICP-MS (Inductively Coupled Plasma Mass Spectrometry) or ICP-OES (Inductively Coupled Plasma Optical Emission Spectroscopy), is an analytical technique used to determine the elemental composition of a sample [42].

3.3.2 Titration tests

Solution titration tests to calculate the concentration of HCO_3^-, $CO_3^{2-}$and OH^-ions were conducted following ASTM D3875 standard "Test Method for Alkalinity in Brackish Water, Seawater, and Brines". These tests are crucial as they provide insights into the water sources buffering capacity and potential for pH fluctuations, which are directly linked to corrosion processes [43].

In these test samples were titrated, using a standardized acid (0.1N), until a pH of 8.1. The volume of acid added was then recorded and denoted with P. In cases where the water being tested has a pH level below 8.1, P was recorded as zero. The titration process was then resumed until the water reached a pH of 4.5. After which the volume of the acid used for the entire process was recorded and denoted with T. Table 5 shows the relation between P and T [44].

Table 5 - Presents the volume relationships necessary for calculating alkalinity [44].

Results	Volume of Standard Acid Corresponding to		
	Bicarbonate HCO_3^-	Carbonate CO_3^{2-}	Hydroxide OH^-
P = 0	T	0	0
$P < \frac{1}{2} T$	T-2P	2P	0
$P = \frac{1}{2} T$	0	2P	0
$P > \frac{1}{2} T$	0	2(T-P)	2P - T
P = T	0	0	T

The formulas to calculate:

HCO_3^- ions: HCO_3^-, mg/L = (A x N x 61 x 1000) / M Eq. (1)

CO_3^{2-} ions: CO_3^{2-}, mg/L = (A x N x 30 x 1000) / M Eq. (2)

OH^- ions: OH^-, mg/L = (A x N x 17 x 1000) / M Eq. (3)

where:

- A = milliliters of acid,
- N = normality of acid,
- M = milliliters of sample.

3.3.3 Quantitative accelerated laboratory evaluation of leached solutions

These tests were done according to standard ASTM C1617 “Standard Practice for Quantitative Accelerated Laboratory Evaluation of Extraction Solutions Containing Ions Leached from Thermal Insulation on Aqueous Corrosion of Metals”. This is a quantitative accelerated laboratory evaluation of extraction solutions containing ions leached from thermal insulation on aqueous corrosion of materials. This test creates the “perfect storm” to induce visual and measurable corrosion through hundreds of wet/dry cycles over 96 hours [45]. The mass loss corrosion rate (MLCR) is determined in mils per year and is called the mass loss corrosion rate (MLCR) [46].

The experiments involved exposing the metal coupons to an extraction solution containing ions leached from thermal insulation for a period of four days.

Each experiment consisted of placing two rectangular AISI 1018 steel samples on a heated plate. The plate was then adjusted to maintain a temperature of 100°C ±5°C. Once the samples reached the desired temperature, leachate solution were delivered to their surfaces

using a peristaltic pump adjusted to dispense 250 mL/day. The experimental setup is show in Figure 15.

Figure 15 - Test coupons are placed on a hot plate and supplied with fluid using a peristaltic pump.

When the test was concluded, samples were cleaned by first scraping the accumulated corrosion by-product, then immersing the sample in concentrated HCl acid. Following the cleaning process, samples were weighed, and the mean rate Mass Loss Corrosion Rate (MLCR) expressed in mils per year was calculated according to:

MLCR = (K x W) / (A x T x D) (mils per year) Eq. (4)

Where:

K = 3.45×10^6 (a constant to convert cm/h to mils/year).

T = time of exposure in h.

A = area of exposure (cm^2); based on the inner radius (cm) of the plastic pipe.

W = mass loss from the coupon (g) = (initial recorded weight of coupon) − (weight of coupon after exposure and cleaning).

D = bulk density of the test metal (g/cm^3).

3.3.4 High temperature electrochemical testing

High temperature electrochemical experiments were conducted in autoclaves following ASTM G189 “Laboratory Simulation of Corrosion Under Insulation” guidelines. The

autoclaves served as controlled test cells, replicating high-pressure and high-temperature environments (Figure 16).

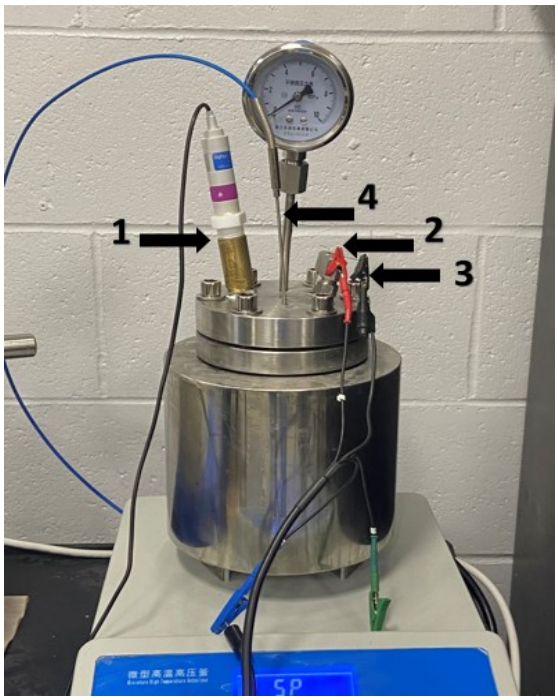

Figure 16 - Autoclave setup

A standard three-electrode setup was utilized for electrochemical testing. The setup consisted of a reference electrode (1), working electrode (2), and a counter electrode (3). A thermocouple placed close to the specimen served to monitor the temperature in the autoclave (4). The working electrode (WE) consisted of an API X52 disk, the counter electrode (CE) of a platinum wire and the reference electrode was saturated Ag/AgCl. Tests were conducted, for a period of 96 hours at 85°C in approximately 350 mL of leachate solution.

3.3.4.1 Potentiodynamic Polarization

Electrochemical potentiodynamic polarization techniques are frequently utilized in corrosion experiments to obtain overall insights into the corrosion resistance and vulnerability of materials. By extrapolating the anodic and cathodic branches of the potentiodynamic polarization curves obtained from linear sweep polarization (LSP) test, corrosion current (I_{corr}) and potential (E_{corr}) values can be found [47].

During testing the working, reference and counter electrodes were connected to a Palmsens potentiostat. Potentiodynamic polarization experiments were performed by applying a potential ramp of 1.667 mV/s to the working electrode, starting at -0.8 v and ending at 0.5 V vs AgCl. Electrochemical parameters necessary to determine the corrosion resistance of the steel were obtained by fitting the curves using the Butler–Volmer Equation:

$$I = i_{corr}(e^{(\ln 10(E-Ecorr)/\beta a)} - e^{-(\ln 10(E-Ecorr)/\beta c)}) \quad \text{Eq. (5)}$$

where i_{corr} is the corrosion current density, it provides valuable insights into the rate at which the electrochemical reactions responsible for corrosion occur on a metal's surface. E_{corr} is the corrosion potential which reflects the thermodynamic tendency of a metal to corrode in a specific environment, "β_a" referred to as the anodic Tafel slope, characterizes the anodic reaction, an essential component of the corrosion mechanism. This reaction involves the dissolution (oxidation) of metal ions from the metal surface. On the other hand, "β_c" known as the cathodic Tafel slope, relates to the cathodic reaction. In this process, reduction reactions occur that consume electrons. These Tafel slopes provide insights into the kinetics of anodic and cathodic reactions. Once the values of β_a and β_c and i_{corr} are known, the Stern–Geary coefficient ($B = \beta_a.\beta_c / (\ln 10 (\beta_a+\beta_c))$) and polarization resistance ($R_p = B/i_{corr}$) can be determined as well.

The corrosion rate can then be calculated using:

$$CR=\frac{kWE}{\rho}\ i_{corr} \quad \text{Eq. (6)}$$

3.3.4.2 Electrochemical impedance spectroscopy (EIS)

EIS tests were conducted in a three-electrode flat corrosion cell shown in Figure 18. The cell consisted of a saturated Ag/AgCl reference electrode (1), an API X52 working electrode (2) and a platinum counter electrode (3). The electrolyte used in this cell consisted of distilled water with a 3.5 w% NaCl. EIS tests were done at OCP, with a 5 mV AC perturbation signal over a frequency range of 0.01 Hz to 50,000 Hz. A pretreatment duration of 600 seconds was employed to allow the sample to reach steady state. All tests were conducted at room temperature and data analysis was done using PSTrace electrochemical package.

The results are presented through two distinct plots: the Nyquist Plot is a graphical way of showing the real and imaginary parts of impedance (Z' and Z'') as coordinates on a plane. This plot helps us understand the electrochemical processes that happen at different frequencies. The Bode Plot is another graphical way of showing the amplitude of impedance on a vertical axis, while the frequency (or angular frequency) is shown on a horizontal axis using a logarithmic scale. The Bode Plot has two graphs, one for amplitude and one for phase angle.

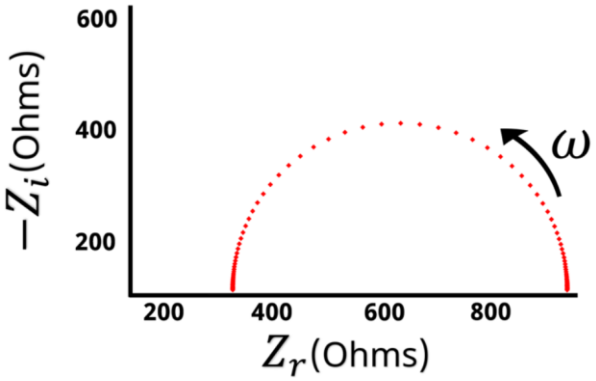

(a)

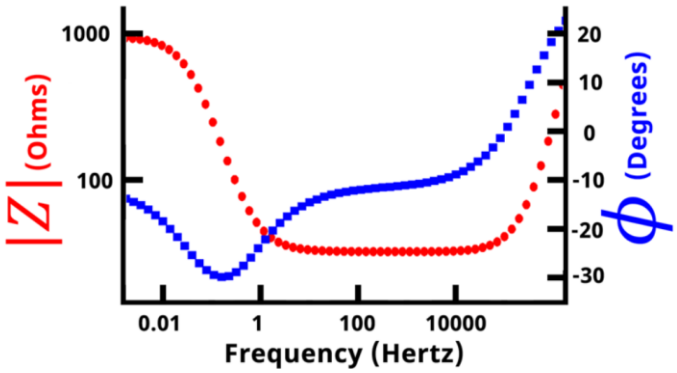

(b)

Figure 17 - Typical EIS test result a) Nyquist spectra and b) Bode plot

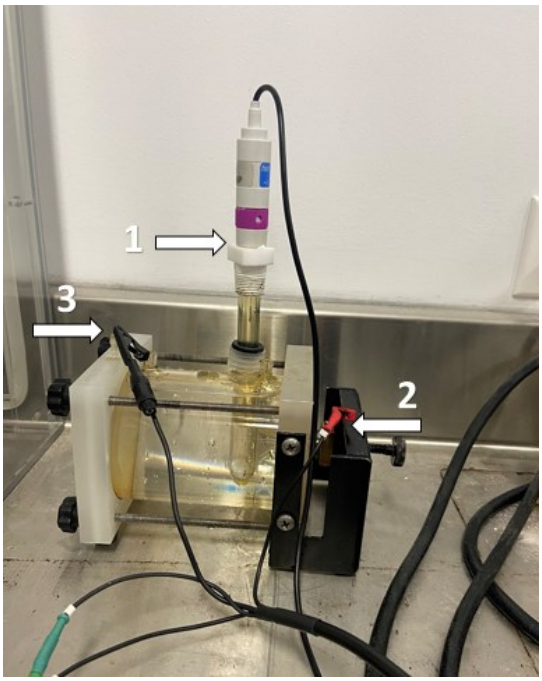

Figure 18 - Corrosion cell for EIS test

3.3.5 Surface characterization

To characterize the surfaces of the corroded X52 and AISI 1018 samples, SEM (Scanning Electron Microscopy), EDS (Energy-Dispersive Spectroscopy), analyses were conducted prior to the removal of the corrosion products [48].

After removal of the corrosion products, samples were cleaned using HCl acid, and examined using a laser confocal microscope at a magnification of 10x, allowing high-resolution imaging, optical sectioning, and detailed three-dimensional images.

3.3.6 Summary of conducted tests

The ensuing Table 6 provides a concise yet comprehensive presentation of the diverse array of tests that have been meticulously undertaken.

Table 6 - Summary of conducted tests

	Perlite insulation	**Mineral wool insulation**
ICP for leachate solutions	6 solutions	6 solutions
Titration solutions	6 solutions	6 solutions
Quantitative accelerated laboratory evaluation of leached solutions	AISI 1018 steel (6 coupons)	AISI 1018 steel (6 coupons)
LSP	X52 steel (6 coupons)	X52 steel (6 coupons)
EIS	X52 steel (6 coupons)	-
Confocal microscope	AISI 1018 steel (6 coupons) & X52 steel (6 coupons)	AISI 1018 steel (6 coupons) & X52 steel (6 coupons)
SEM & EDS	X52 steel (6 coupons)	X52 steel (6 coupons)

Chapter 4: Results and discussions

In this pivotal chapter, the results of the experimental work as well as their discussion is presented.

4.1 Perlite leachate solutions

Leachate solutions for perlite aged for 0, 45 and 90 days were prepared according to ASTM C871. ICP was used to determine the alkali ions concentrations and titration was used to determine HCO_3^-, $CO_3^{2-}$and OH^-concentrations.

4.1.1 ICP of the perlite leachate solutions

The ICP analysis of the 20 and 80g leachate solution is presented in figure 19.

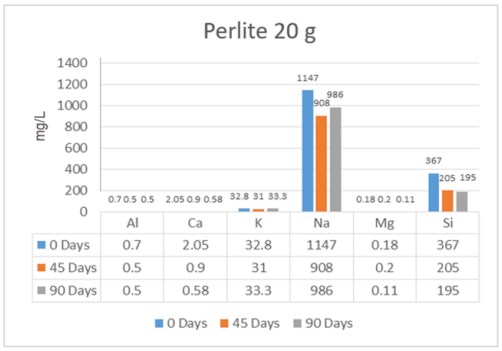

(a)

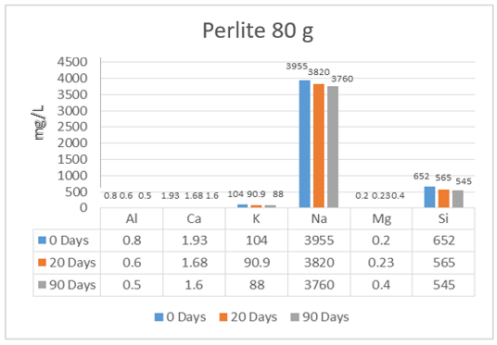

(b)

Figure 19 - ICP analysis was conducted to determine the concentrations (in mg/L) of alkali elements + Al in perlite leachate solutions obtained from insulation samples that were aged at 150°C in a furnace for 0-, 45-, and 90-days a) 20g, b) 80g

As can be seen from Figure 19-a, a significant high concentration of Na is evident in all the leachate solution. Measuring approximately 1150 mg/l for the pristine insulation (0-day). However, after subjecting the insulation to a burning process for 45 and 90 days, the concentration decreased to around 900 mg/l and 986 mg/l, respectively.

It is worth mentioning that the concentrations of the other elements (Al, Ca, K, Mg, and Si) remained relatively stable throughout this process. Similarly, a high concentration of Na is observed in (80g) leachate solution compared to other elements, with initial concentration of approximately 3955 mg/l. However, following a burning process of 45 and 90 days, the concentration decreased to approximately 3820 mg/l and 3760 mg/l, respectively.

During the aging process, both the (20g) and (80g) leachate solutions show a slight decrease in the concentration of alkali elements. When perlite insulation is combusted, alkali elements are released as gases or vaporized particles. These gases and particles are carried away by the combustion products, causing a decline in their concentration within the burned material [49], [50].

The decrease of Na can be attributed to certain chemical reactions occurring in the solution [49], [51], [52],[53], such as:

$2\ Na_2O + 3CO_2 \rightarrow Na_2CO_3.$ (Reaction 1)

Where two molecules of sodium oxide react with three molecules of carbon dioxide to produce one molecule of sodium carbonate [54].

$Na + H_2O \rightarrow NaOH + H_2.$ (Reaction 2)

The majority of the resulting product from the reaction, sodium hydroxide (NaOH), is expected to be in a liquid state [55].

4.1.2 Titration tests

Leachate solutions for mineral wool aged for 0, 45 and 90-days were prepared according to ASTM C871 guidelines. ICP was used to determine the alkali ions concentrations and titration was used to determine HCO_3^-, $CO_3^{2-}$and OH^-concentrations.

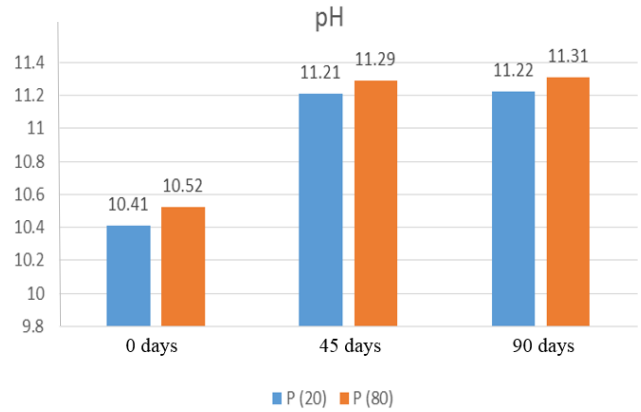

Figure 20 - pH of perlite leachate solutions 20g and 80g obtained from insulation samples that were aged at 150°C in a furnace for 0-, 45-, and 90-days

The pH of the perlite leachate solutions followed an upward trend with aging time and increased insulation weight as shown in Figure 20. This incremental change is most likely due to the increase in the $CO_3^{2-}$and OH^- ions as seen in Figure 21 & Figure 22.

The pH level of the leachate solution plays a crucial role in the initial dissolution of some elements in alkali solutions. Studies have shown that solutions with a higher pH are effective in promoting the dissolution of these elements. On the other hand, solutions with a pH below 9.5 do not facilitate the dissolution and reaction of these elements [56]. Hence, this will explain the decrease in the alkali elements shown in Figure 19.

Titration tests were performed on two separate occasions to ensure accuracy, and the resultant average value is meticulously displayed in Table 7 & Table 8 , accompanied by the corresponding percentage error.

Table 7 - The mean concentration of CO_3^{2-} ions in perlite leachate solutions determined through titration, along with the corresponding errors

Solution	**0 - 20**		**0 – 80**		**45 - 20**		**45 - 80**		**90 - 20**		**90 - 80**	
	mg/L	Err	mg/L	Err	mg/L	Err	mg/L	Err	mg/L	Err	mg/L	Err
CO_3^{2-}	1284	3%	4236	3.6%	1416	4%	4440	2.8%	1420	2%	4516	2.2%

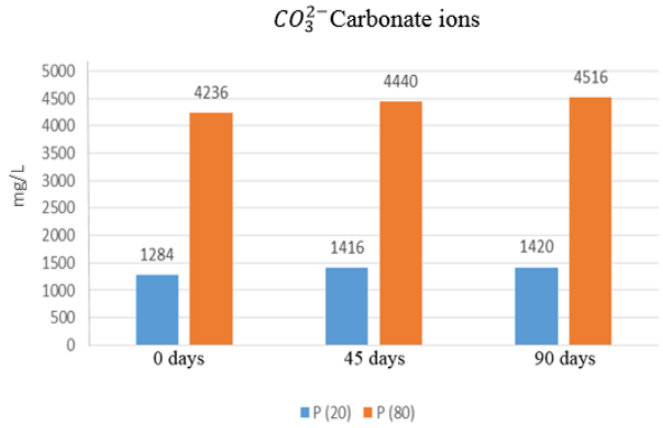

Figure 21 - Concentration of carbonate ions (CO_3^{2-}) in (mg/L) in perlite leachate solutions 20g and 80g solutions obtained from insulation samples that were aged at 150°C in a furnace for 0-, 45-, and 90-days

Table 8 - The mean concentration of OH^- ions in perlite leachate solutions determined through titration, along with the corresponding errors

Solution	**0 - 20**		**0 – 80**		**45 - 20**		**45 - 80**		**90 - 20**		**90 - 80**	
	mg/L	Err	mg/L	Err	mg/L	Err	mg/L	Err	mg/L	Err	mg/L	Err
OH^-	64.6	2%	115.6	3%	133.9	1.5%	306	4%	149.6	4%	557.6	3%

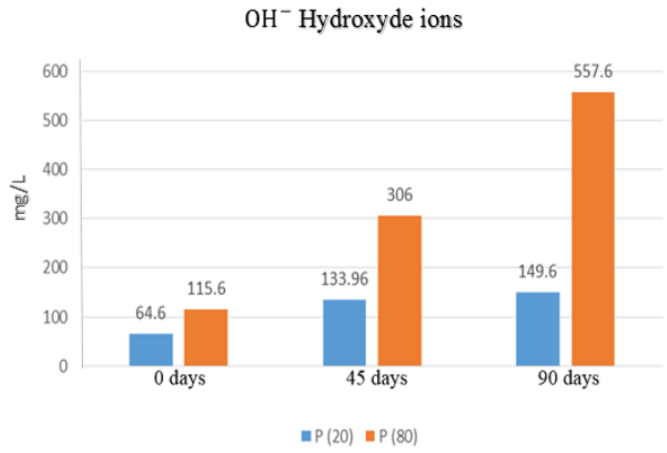

Figure 22 - Concentration of OH^- in (mg/L) in perlite leachate solutions 20g and 80g solutions obtained from insulation samples that were aged at 150°C in a furnace for 0-, 45-, and 90-days

After aging perlite insulation, the leachate solution might experience an elevation in CO_3^{2-} and OH^- ions owing to various factors Figure 22. Among these factors is the potential decomposition of both organic and inorganic substances found within the perlite insulation. Such decomposition can liberate carbon dioxide gas, which subsequently dissolves in water, resulting in the formation of CO_3^{2-}[49],[51]. Moreover, as the aging process progresses, there is a possibility of alkaline hydroxide and some compounds containing CO_3^{2-} being leached from the perlite material. Furthermore, the formation of $CO_3^{2-}$and OH^- ions in the leachate solution of aged perlite can be related to the reactions mentioned previously between Na with CO_2 and H_2O (Reactions 1&2).

The calculated concentration of HCO_3^- ions as derived from the data in Table 5, is determined to be zero.

4.1.3 Quantitative accelerated laboratory evaluation of leached solutions

Quantitative accelerated laboratory evaluation tests were done following ASTM 1617 guidelines.

4.1.3.1 Mass Loss Corrosion Rate

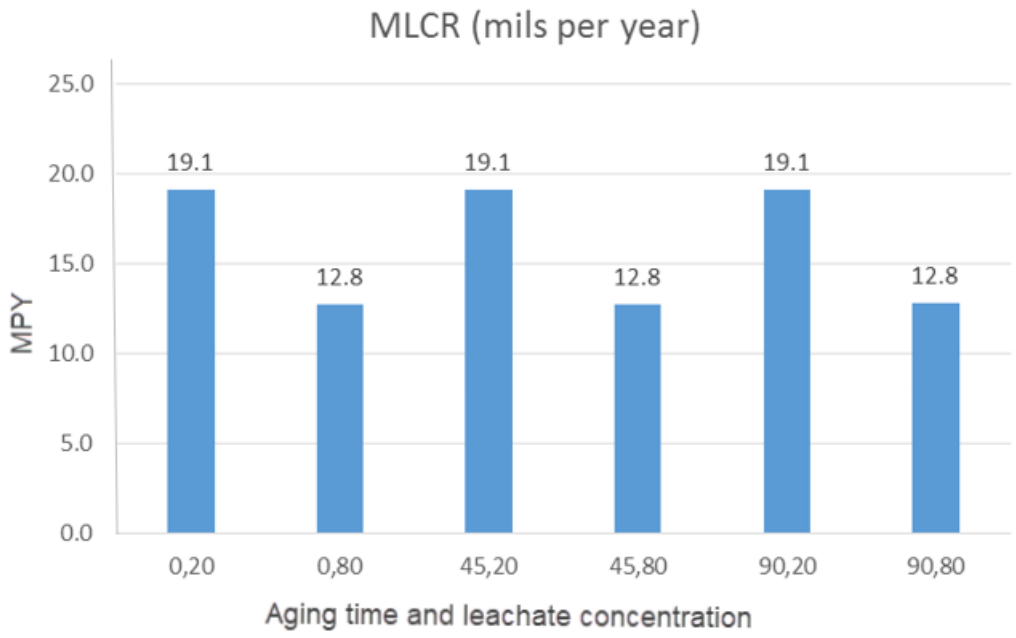

Figure 23 - Mass Loss Corrosion Rate (MLCR) for mineral wool leachate solutions.

As can be seen from Figure 23, the MLCR for samples exposed to 20g pearlite leachate solutions, aged for 0, 45 and 90 days, exhibited a weight reduction of about 0.03g, whereas the samples tested with the 80g solutions experienced a slight decrease of about 0.02g. Based on the MCLR rates, it is evident that the corrosion occurring under perlite insulation is significantly reduced with an increase in the perlite concentration. Despite the overall lower corrosion rates observed, it is noteworthy that the samples exposed to the 20g leachate solutions exhibited a higher level of uniform and pitting corrosion compared to the ones exposed to the 80g solutions. Therefore, increasing the concentration of perlite leads to a corresponding rise in the presence of OH^- ions and CO_3^{2-}within the solution

coupled with an elevated pH, as a result, the corrosion rates and associated symptoms can be effectively reduced.

5.1.3.2 Confocal laser microscopy

To further assess the impact of the aforementioned leachate solutions on the steel coupons, confocal laser microscopy surface characterization was employed.

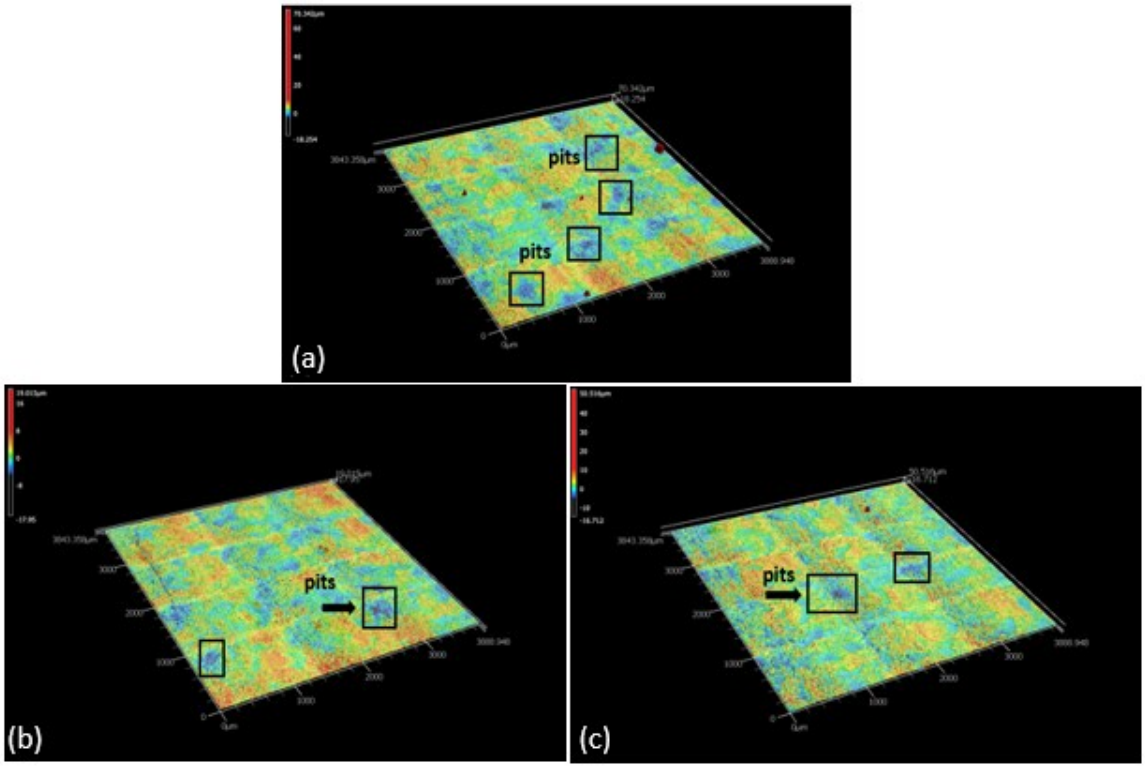

Figure 24 - Confocal laser microscope images of (4 mm x 4 mm scan area) surface of AISI 1018 steel exposed to 20g perlite leachate solutions obtained from insulation samples that were aged at 150°C in a furnace for a) 0-, b) 45-, and c) 90-days

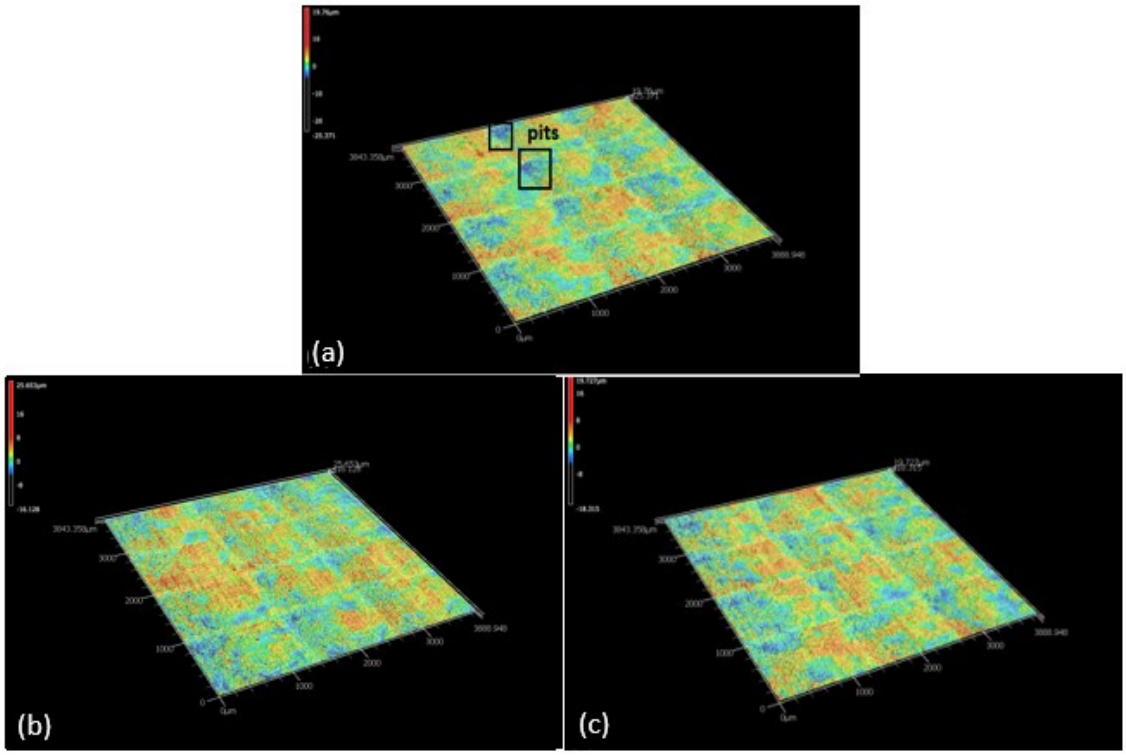

Figure 25 - Confocal laser microscope images of (4 mm x 4 mm scan area) surface of AISI 1018 steel exposed to 80g perlite leachate solutions obtained from insulation samples that were aged at 150°C in a furnace for a) 0-, b) 45-, and c) 90-days

As shown in Figure 24 & Figure 25, the 3D micrographs captured with a confocal microscope reveal a noticeable reduction in pitting corrosion. This decrease occurs with both the aging process and the concentration of the leachate solution.

This reduction can be attributed to the formation of an extremely thin layer of corrosion product (passive film) on the surface of the metal, which acts as a barrier against further chemical reactions when perlite solutions are utilized. This film acts as a protective layer, effectively safeguarding the surface against corrosion and is often invisible to the naked eye [57].

Passive films are generally formed when a bare metal surface is exposed to an oxidizing environment. Once the film is formed, the rate of reaction between the metal and the surrounding environment decreases significantly, often by several orders of magnitude [58] [59]. However, these passive films are often vulnerable to localized breakdown, which can result in the accelerated dissolution of the underlying metal when corrosion attack begins on an exposed surface [60] [61].

4.1.4 High temperature electrochemical testing

Two types of electrochemical testing were done to assess the corrosion behaviors of steels samples exposed to 20g and 80g perlite leachate solutions.

4.1.4.1 Potentiodynamic polarization tests

The changes in corrosion resistance were quantitatively assessed using linear sweep polarization (LSP) and the resulting data were plotted using potentiodynamic curves shown in Figure 26 and Figure 27. The resulting electrochemical parameters E_{corr}, I_{corr}, CR and R_p, which were extracted from these plots using Tafel extrapolation, are displayed in corresponding Tables 9 - 14. The corrosion potential E_{corr} represents the thermodynamic measure that indicates the material's susceptibility to corrosion in a specific environment. Consequently, the corrosion tendency of the tested material diminishes with higher values of E_{corr} and vice versa.

Perlite solutions 20 g:

Potentiodynamic plots were generated using a potential range of -0.8 to +0.5 V vs OC and a scan rate of 0.1667 mV/s.

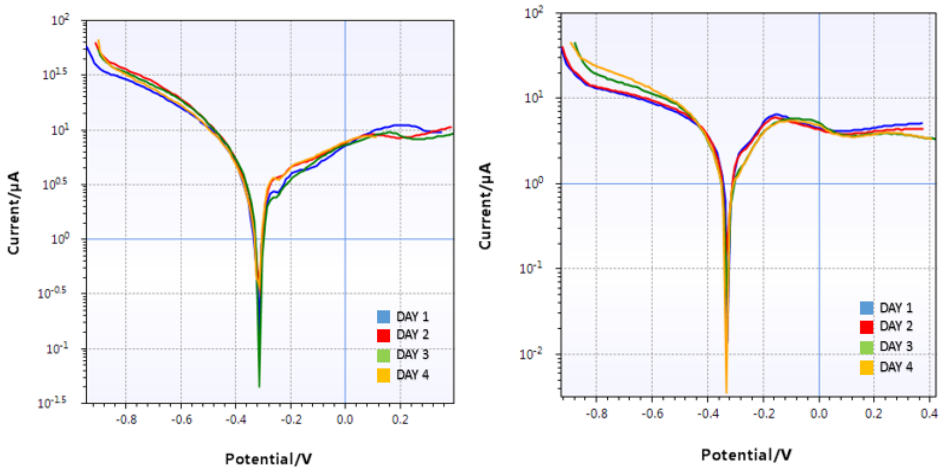

(a) (b)

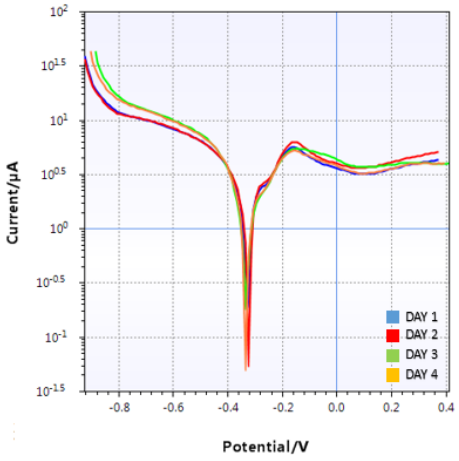

(c)

Figure 26 - Potentiodynamic polarization curves were obtained for the API X52 steel electrodes immersed in 20g perlite leachate solutions obtained from insulation samples that were aged at 150°C in a furnace for a) 0-, b) 45-, and c) 90-days

Table 9 - Corrosion parameters extracted from potentiodynamic polarization curves measured over 4 days for API X52 electrodes immersed in perlite, 0 days, 20g leachate solution.

P - 0 days -20g	E_{corr} (V)	I_{corr} (µA)	Rp (KΩ)	CR (mm/year)
Day 1	-0.316	56.16	18.35	0.33
Day 2	-0.312	9.665	18.25	0.06
Day 3	-0.314	9.532	25.8	0.06
Day 4	-0.314	7.539	21.11	0.04

Table 10 - Corrosion parameters extracted from potentiodynamic polarization curves measured over 4 days for API X52 electrodes immersed in perlite, 45 days, 20g leachate solution

P - 45 days -20g	E_{corr} (V)	I_{corr} (µA)	Rp (KΩ)	CR (mm/year)
Day 1	-0.332	43.65	25	0.25
Day 2	-0.332	25.69	25.66	0.15
Day 3	-0.328	13.03	26.69	0.08
Day 4	-0.327	5.759	27	0.03

Table 11 - Corrosion parameters extracted from potentiodynamic polarization curves Figure 46 measured over 4 days for API X52 electrodes immersed in perlite, 90 days, 20g leachate solution.

P - 90 days -20g	E_{corr} (V)	I_{corr} (µA)	Rp (KΩ)	CR (mm/year)
Day 1	-0.335	31.28	26.25	0.18
Day 2	-0.337	24.05	26	0.14
Day 3	-0.325	5.747	26.2	0.03
Day 4	-0.325	5.361	26.7	0.03

As can be seen from Table 9, 7 and 8, the value of E_{corr} increases with increasing insulation aging time, thus the steel samples resistivity to corrosion increases. This is most likely due to the fact that aged insulation, leaches more ions over time, resulting in solutions rich in

$CO_3^{2-}$and OH^- (Figure 21, Figure 22). These in turn might contribute to the formation of a thin, invisible passive layer, that protects the surface of the samples from further corrosion. This is in complete agreement with the changes in the values of I_{corr}, which are decreasing with increasing insulation aging time, suggesting that the corrosion rate is decreasing due to the formation of this passive layer. This behaviour is also supported by Eq. (5) where the corrosion current density (i_{corr}) is directly proportional to the corrosion rate (CR) calculated using Eq. (6). Notably, the values of E_{corr}, I_{corr}, and CR collectively indicate that an increasing the insulation aging time, which in turn increases concentration of $CO_3^{2-}$and ions in the leachate solution decelerates the corrosion of API X52. However, a decrease in both the E_{corr} and I_{corr} can be observed over the four days span. The decrease in E_{corr} is most likely due to the consumption of dissolved oxygen in the leachate solution. Thus slowing down the cathodic reaction rate.Whereas the decrease in I_{corr} could be attributed to the thickening of the passive layer, which increases the protection of the steel surface.

Perlite solutions 80 g:

The potentiodynamic plot for steel samples exposed to the 80 g perlite solution aged for 0, 45 and 90 days are shown in Figure 27 and the extracted electrochemical parameters are shown in Tables 12, 13 and 14.

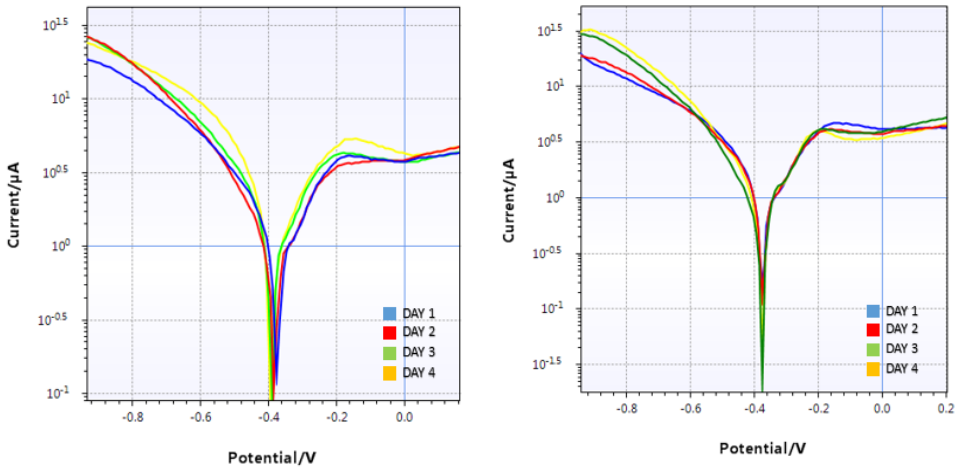

(a) (b)

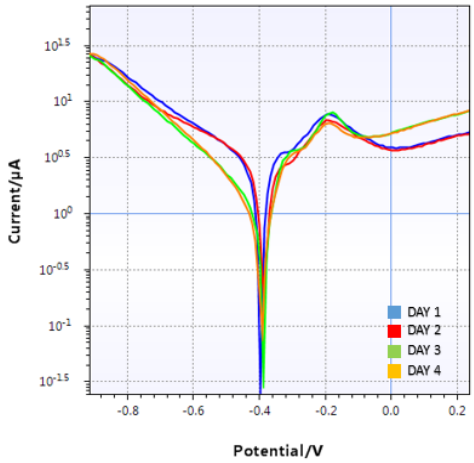

(c)

Figure 27 - Potentiodynamic polarization curves were obtained for the API X52 steel electrodes immersed in 80g perlite leachate solutions obtained from insulation samples that were aged at 150°C in a furnace for a) 0-, b) 45-, and c) 90-days

Table 12 - Corrosion parameters extracted from potentiodynamic polarization curves measured over 4 days for API X52 electrodes immersed in perlite, 0 days, 80g leachate solution.

P - 0 days -80g	**E_{corr} (V)**	**I_{corr} (µA)**	**Rp (KΩ)**	**CR (mm/year)**
Day 1	-0.394	12.55	32.33	0.07
Day 2	-0.389	11.93	36.92	0.07
Day 3	-0.385	5.46	44.74	0.03
Day 4	-0.377	5.228	44.06	0.03

Table 13- Corrosion parameters extracted from potentiodynamic polarization curves measured over 4 days for API X52 electrodes immersed in perlite, 45 days, 80g leachate solution.

P - 45 days -80g	E_{corr} (V)	I_{corr} (µA)	R_p (KΩ)	CR (mm/year)
Day 1	-0.376	11.72	40.93	0.07
Day 2	-0.377	5.582	42.86	0.03
Day 3	-0.375	5.228	44.06	0.03
Day 4	-0.372	3.183	53.6	0.02

Table 14 - Corrosion parameters extracted from potentiodynamic polarization curves measured over 4 days for API X52 electrodes immersed in perlite, 90 days, 80g leachate solution.

P - 90 days -80g	E_{corr} (V)	I_{corr} (µA)	R_p (KΩ)	CR (mm/year)
Day 1	-0.396	8.379	20	0.05
Day 2	-0.392	6.119	23.9	0.04
Day 3	-0.389	2.645	31.22	0.02
Day 4	-0.388	2.451	73.6	0.01

As can be seen from the electrochemical parameters' values, I_{corr} followed a decreasing trend for both insulation aging time (0, 45 and 90 days) and steel exposure time (4 days). Also, the I_{corr} values of the steel samples exposed to the 80 g solution were considerably lower than those obtained for steel samples exposed to the 20 g solution. This is expected due to the higher concentration of CO_3^{2-} and OH^- ions in the 80 g solution, which might lead to the formation of a thicker passive layer, hindering further dissolution of the steel samples. R_p followed an increasing trend with the steel samples' exposure time and that due to the formation of the passive layers and its thickening over the period of the test. Furthermore, R_p values for the samples exposed to the 80 g solution were considerably higher than those for the samples exposed to the 20 g solution and this again is due to the thicker passive layer forming in the latter solution due the abundance of the CO_3^{2-} and

OH^- ions. E_{corr} adhered to the anticipated declining pattern as the samples were exposed to the solution over time. This is attributed to the reduction in dissolved oxygen in the solution. Conversely, the potential exhibited an increasing trend with increasing insulation aging time, attributable to the thickening of the passive layer. Nevertheless, an unanticipated drop occurred for samples exposed to the 45-day aged solution compared to those exposed to the 0-day aged solution then it increased for the 90-day aged solutions. This could potentially be attributed to the excessive concentration of CO_3^{2-} ions. If the concentration of CO_3^{2-} in the solution becomes very high, it can lead to the overgrowth or over-accumulation of the protective carbonate scale. The overgrown scale may become less adherent to the metal surface or develop microscopic pores, cracks, or defects. These changes can weaken the integrity of the scale and create pathways for corrosive agents to reach the metal substrate so lead to the decrease of E_{corr} [62].

Samples in solutions with the same insulation aging time but different concentrations, such as Table 9 & Table 12, Table 10 & Table 13 , and Table 11 & Table 14, I_{corr} values were lower in the 80 g solution, while the polarization resistances were higher, indicating a decrease in the corrosion rate and an enhancement of the steel's nobility in the 80 g solution. This leads to the same conclusion previously drawn those solutions with higher concentrations of CO_3^{2-} and OH^- ions exhibit better resistivity against corrosion due to the formation of a thin passive layer on the surface of the substrate.

Table 12, & Table 14 show the electrochemical parameters (I_{corr}, E_{corr}, R_p) for samples exposed to the 80 g solution at different insulation's aging times 0, 45, and 90 days, respectively. It is evident that as the aging time of the insulation increases, the resistivity to corrosion also increases. This is due to the fact that the insulation, leaches more ions with increasing aging time, resulting in leachate solutions rich in $CO_3^{2-}$and OH^- ions (Figure 21, Figure 22).

This is further emphasized by the composition of the perlite leachate solutions, which contains substantial amount of OH^- and CO_3^{2-}. According to F. F. Eliyan, CO_3^{2-} ions play a direct role in the oxidation process, leading to the formation of iron carbonate ($FeCO_3$). $FeCO_3$ is formed simultaneously with $Fe(OH)_2$, and the formation of $Fe(OH)_2$ is driven by OH^- ions, which increase the local alkalinity and facilitate the initial stages of dissolution.

Additionally, CO_3^{2-}can directly react with Fe^{2+} ions, resulting in different outcomes depending on the solubility limits [63].

During the process of passivation, the film composed of CO_3^{2-} undergoes a transformation into a reactive layer. This reactive layer exhibits oxidation behavior at higher potentials when subjected to a forward scan in the presence of O_2 and OH^-. Consequently, the passive film undergoes thickening and experiences a change in its chemical composition. This thickening is accompanied by the formation of iron oxides, resulting in a multilayered passive film. The electrochemical generation of $Fe(OH)_2$ is thermodynamically more favorable than the formation of $FeCO_3$ at the initial stages. An increase in CO_3^{2-} concentration leads to an augmentation in dissolution and consequent precipitation of $FeCO_3$. Additionally, the reactivity of $FeCO_3$ in transitioning into iron oxides is heightened. Consequently, the passive films become thicker, suppressing the dissolution underneath while simultaneously exhibiting higher reactivity [63].

Moreover, the effect of temperature and CO_3^{2-} concentrations have a considerable effect on the passivity of the steel. Raising the temperature not only intensifies the process of dissolving the steel substrate but also facilitated the formation of $FeCO_3$, which is the primary product of corrosion. As for the concentration of CO_3^{2-} increases, the corrosion rate decreased.

This behavior is most likely due to an increase in the solution's pH with an increase in the concentration of CO_3^{2-}. For pH values larger than 9, the formation of $Fe(OH)_2$ is thermodynamically favored. Given that the leachate solution is rich in both $CO_3^{2-}$and OH^- ions, this conclusion is very plausible and in agreement with previously done work by , Artamonova et al [63], [64]. In their work on steel passivation, they found that there exist two distinct regions for the dependence of corrosion rate on pH. They proposed that when the pH values are lower than 9, there is no significant correlation between its values and the corrosion rate, whereas when the pH values are larger than 9, there is a sharp decrease in the corrosion rate, which infers that as the pH increases, the corrosion rate decreases. The researchers also indicate that an increase in the oxygen concentration leads to an increase in the corrosion rate. They further suggest that ions such as CO_3^{2-}or OH^- have a notable influence on the corrosion rate of steel. They observe that in the presence of low

concentrations of CO_3^{2-}, the corrosion rate actually increases, and the same trend is observed for OH^-[64].

Furthermore, to strengthen this notion, Gil et al. conducted a study comparing the current densities of aged X52 steel samples tested in carbonate-containing solutions. The results shown in Figure 28, show a considerable drop in the corrosion rate of the steel with an increase in the concentration of CO_3^{2-} from 0.01 M to 0.1 M [65].

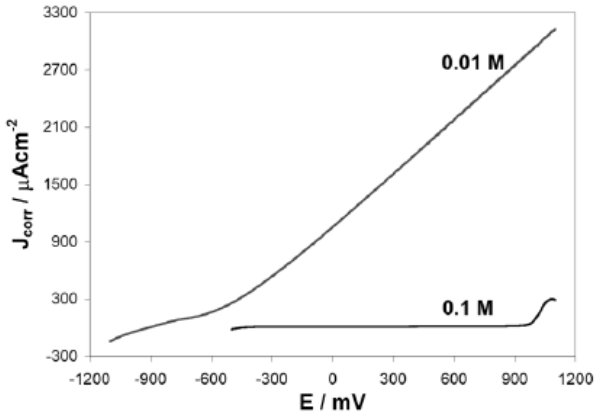

Figure 28 - The electrochemical characteristics of the X52 samples submerged in aqueous solutions of $NaHCO_3$ with two distinct concentrations are illustrated in the figure [65].

4.1.4.2 Electrochemical Impedance Spectroscopy

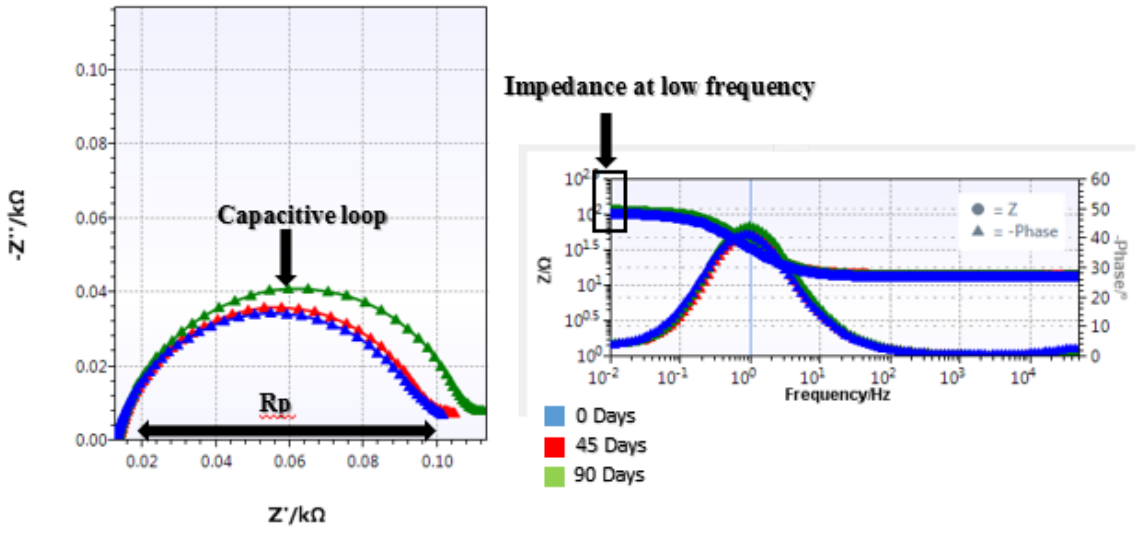

(a) (b)

Figure 29 - Electrochemical Impedance Spectroscopy curves were obtained for the API X52 steel electrodes immersed in 20g perlite leachate solutions aged for 0-, 45-, and 90-days, a) Nyquist Plot and b) Bode Plot.

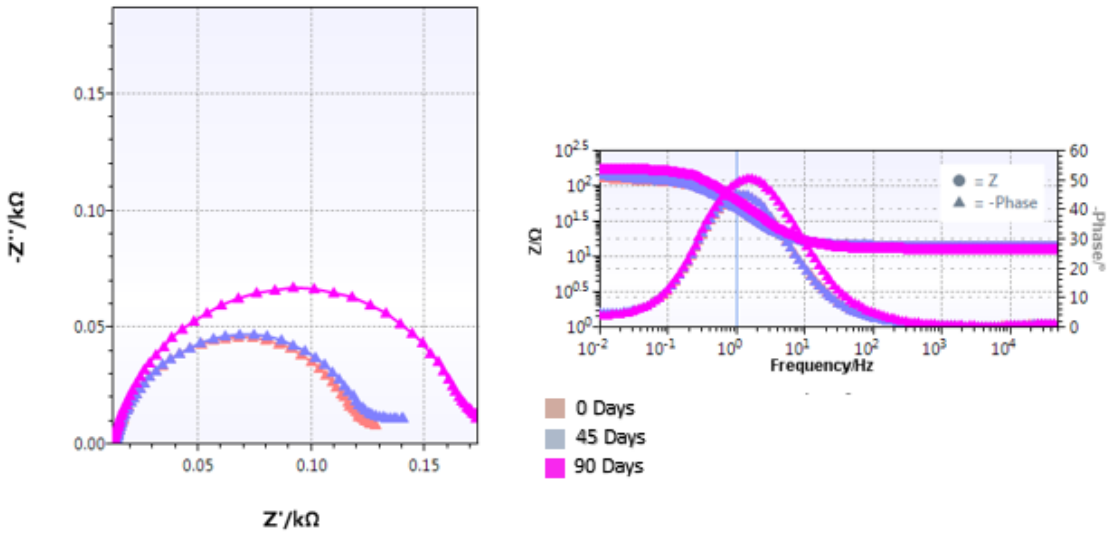

(a) (b)

Figure 30 - Electrochemical Impedance Spectroscopy curves were obtained for the API X52 steel electrodes immersed in 80g perlite leachate solutions aged for 0-, 45-, and 90-days, a) Nyquist Plot and b) Bode Plot

Figure 29 & Figure 30 show the Nyquist and Bode plots for steel samples exposed to the 20 g and 80 g perlite leachate solutions, respectively. As can be seen from the Nyquist plot of the 20g perlite solution, there is a clear increase in the R_p values from 0.105 to 0.128 kΩ, which is indicative of an increase in the corrosion resistance of the steel with an increase in the aging time of the insulation. This agrees with the LSP data shown in **section 4.1.4.1.** Accompanying this increase in R_p is an increase in the capacitive loop, which indicates a thickening of the passive layer forming on the surface of the steel which will result in a lower corrosion current, thus a lower corrosion rate.

Upon comparing the R_p for the steel samples exposed to the 20 g and 80 g pearlite leachate solutions, it can be seen that for 80 g solution, the magnitude of R_p is higher than that of steel samples exposed to the 20 g solution for same aging period. This is an indication that the increase in the concentration of perlite, causes an increase in the corrosion resistance of the steel, which is also in agreement with the result of the LSP experiments and it is due to the increase in both the $CO_3^{2-}$and the OH^-. Moreover, there is a considerable increase in the capacitive loop as compared to the steel samples exposed to the 20 g perlite solution for the same aging time and this is due to an increase in the thickness and compaction of the passive layer over the one formed in the 20 g solution.

The increase in the corrosion resistance of the steel with increasing aging time and perlite concentration is further reinforced by the increase of the impedance of the steel surface as shown in the low frequency range on the Bode plot.

4.1.5 Surface characterization

Autoclave steel samples were examined for surface corrosion using confocal laser microscopy. The images are shown in Figure 31 and Figure 32. Blue areas indicate depressed or corroded regions. Whereas dark orange areas indicate pristine or uncorroded regions. The deeper the blue color, the more significant the extent of corrosion is.

4.1.5.1 Confocal laser microscopy

Confocal laser microscopy was done at 10x magnification to allow for a clear view of the surface features.

Perlite solutions 20 g:

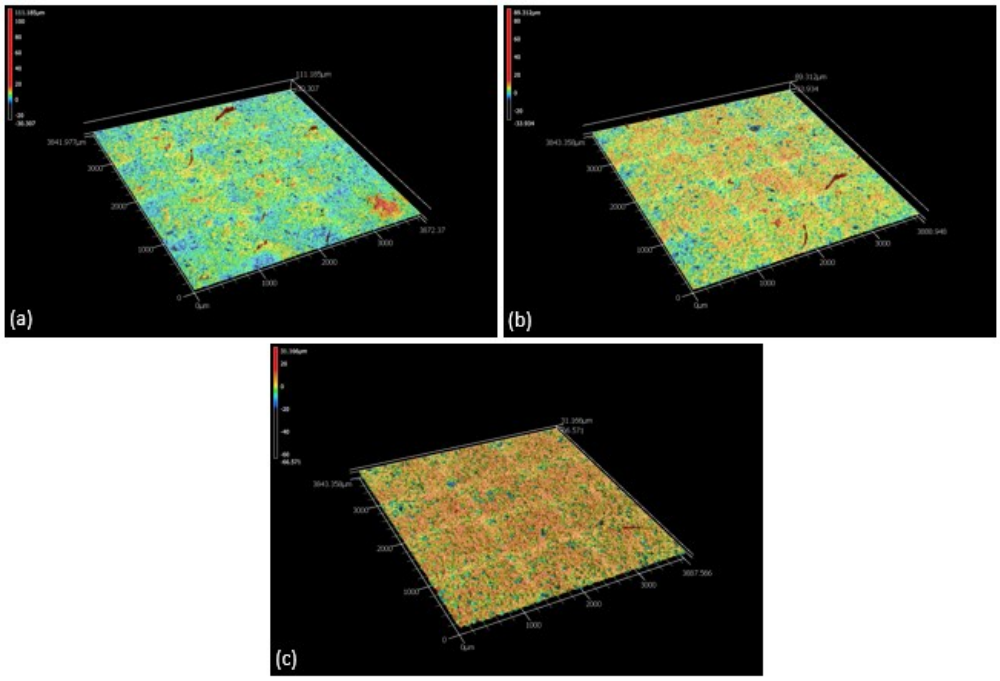

Figure 31 - Confocal laser microscope images of (4 mm x 4 mm scan area) surface of API 5L grade X52 steel tested for 4 days in the autoclave containing 20g perlite leachate solutions obtained from insulation samples that were aged at 150°C in a furnace for a) 0- , b) 45-, and c) 90-days

As can be seen, from Figure 31-a, the surface of the steel subjected to the leachate solution from the pristine insulation (0-day), showed considerable localized corrosion in the form of pits, which according to Cao et al, is the most likely form of corrosion to occur when steels are exposed to alkaline solutions [23]. For the steel samples subjected to the leachate solution from the 45-days aged perlite insulation, Figure 31-b, the number of pits decreased considerably in comparison to the surface of the steel subjected to the leachate solution from the pristine insulation, and that is in agreement with the electrochemical data presented in the section 4.1.4.1 of this thesis. Steel samples that were exposed to the leachate solution from the 90-days aged insulation, Figure 31-c, showed minimal localized corrosion and that again agrees with the previously presented electrochemical data.

Perlite solutions 80 g:

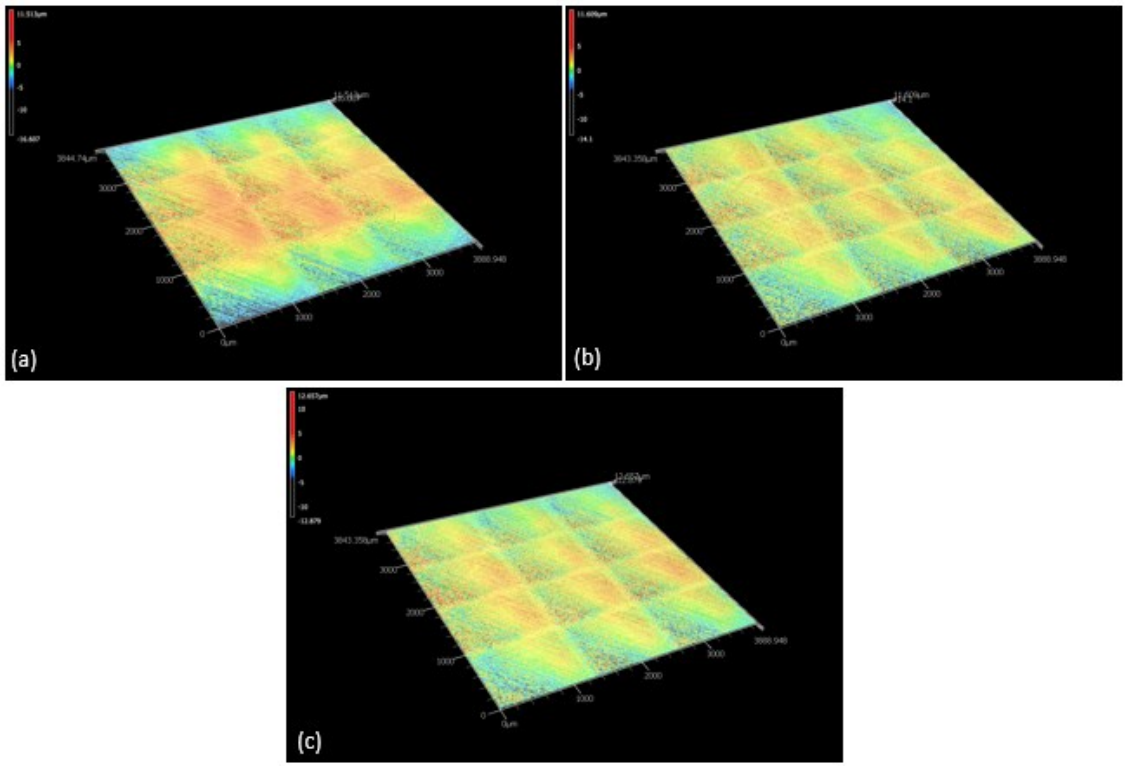

Figure 32 - Confocal laser microscope images of (4 mm x 4 mm scan area) surface of API 5L grade X52 steel tested for 4 days in the autoclave containing 80g perlite leachate solutions obtained from insulation samples that were aged at 150°C in a furnace for a) 0- , b) 45-, and c) 90-days

Steel samples exposed to the leachate solution containing 80g perlite solution showed a considerably lower susceptibility to corrosion compared to the samples exposed to the 20g perlite leachate solution. As can be seen from Figure 32- a,b,c, the surface of the steel showed minimal signs of corrosion as indicated by the presence of the blue areas in the confocal laser microscope images. In comparing the six corroded samples in Figure 31 & Figure 32, a notable trend emerged, showing a decrease in corrosion with increase in the concentration of the perlite insulation in the solution and the aging period. Both observations are corroborated by the electrochemical results presented section 4.1.4.1. This phenomenon could be attributed, as mentioned previously, to the alkaline nature of the perlite insulation, which promotes passivation by both raising the pH, which encourages the formation of $Fe(OH)_2$, and forming a thin layer $FeCO_3$ due to its high CO_3^{2-}content [66] ,[67].

4.1.5.2 SEM & EDS

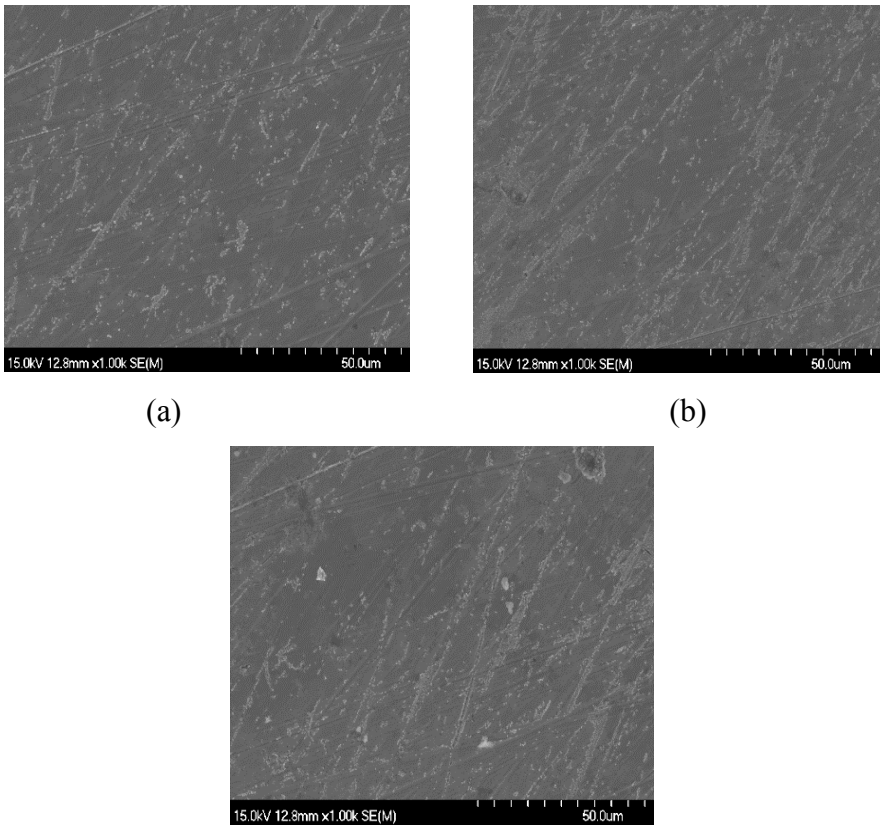

(a) (b)

(c)

Figure 33 - Scanning electron microscope (SEM) micrographs of the surface of X52 steel tested in the autoclave containing 20g perlite leachate solutions obtained from insulation samples that were aged at 150°C in a furnace for a) 0-, b) 45-, and c) 90-days

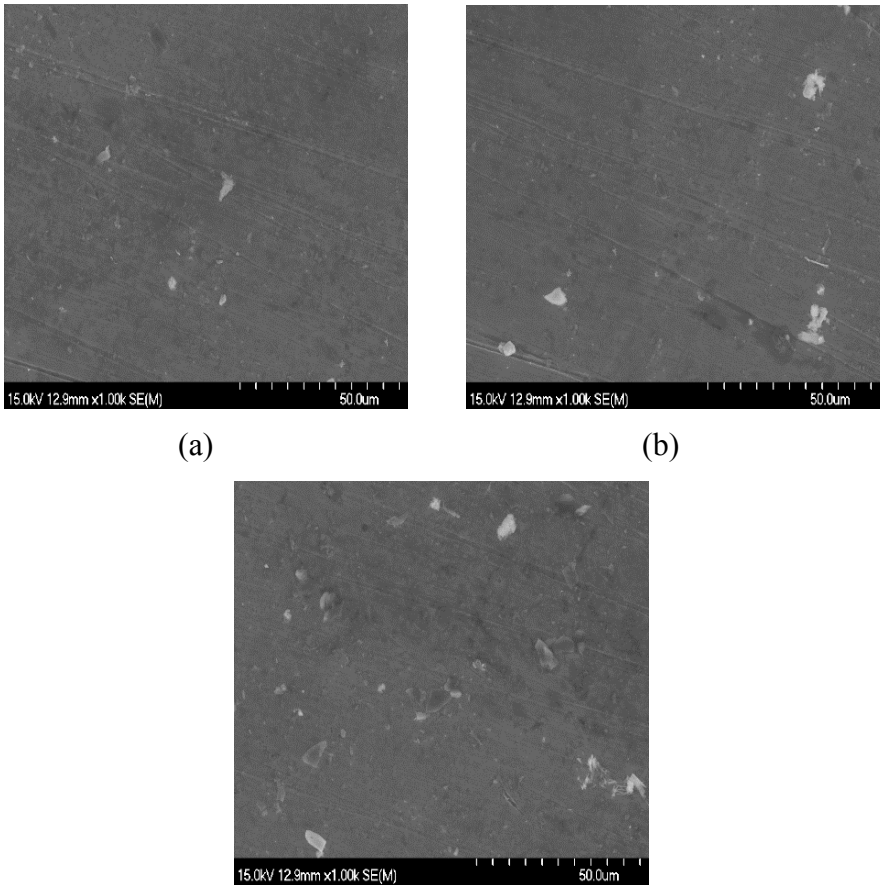

(a) (b)

(c)

Figure 34 - Scanning electron microscope (SEM) micrographs of the surface of X52 steel tested in the autoclave containing 80g perlite leachate solutions obtained from insulation samples that were aged at 150°C in a furnace for a) 0-, b) 45-, and c) 90-days

SEM micrographs of the surface of the autoclave samples exposed to the 20 g and 80 g perlite leachate solutions, are shown in Figure 33 and Figure 34. As can be seen the samples did not show any visible corrosion products or significantly corroded areas on their surfaces. This was expected as the most likely corrosion product was a thin composite layer of $Fe(OH)_2$ and $Fe(CO)_3$, which is very thin and transparent. EDS data presented in Table *15* further supported these findings, as they showed a rise in the weight% of oxygen and carbon, attributed to the layer's formation, along with a decline in the weight percentage of iron, which could be attributed to the layer's thickening and obstructing the analysis of the surface. The same trend is observed for samples exposed to the 80 g perlite leachate solution.

Table 15 - The results of the Energy Dispersive Spectroscopy (EDS) analysis on the corrosion products of the API X52 steel sample immersed in a perlite leachate solutions.

Elements (% weight)	C	O	Na	Si	Mn	Fe	Total
P - 0 - 20	3.27	1.55	0.41	0.51	0.6	93.66	100
P - 45 - 20	3.33	1.87	0.4	0.59	0.58	93.23	100
P - 90 - 20	3.91	2.54	1.19	0.64	0.6	91.12	100
P - 0 - 80	3.7	4.28	0.63	1.74	0.67	88.98	100
P - 45 - 80	3.85	4.51	0.64	1.66	0.7	88.64	100
P - 90 - 80	4.16	5.61	1.17	2.16	0.64	85.71	100

Comparing the composition of the layers that formed on the steel samples exposed to the 0, 45 and 90-days 80 g leachate solutions, a slight increase in the weight percentage of carbon (C), oxygen (O), and a decrease in the weight percent of iron (Fe) were observed with an increase in the insulation aging period. This is attributed to the thicker passive layer forming on the surface of the steel samples, due to the increase in CO_3^{2-} and OH^- in the leachate solution.

4.2 Mineral wool leachate solutions

4.2.1 ICP of the mineral wool leachate solutions

Leachate solutions for mineral wool aged for 0, 45 and 90-days were prepared according to ASTM C871 guidelines. ICP was used to determine the alkali ions concentrations and titration was used to determine HCO_3^-, $CO_3^{2-}$and OH^-concentrations.

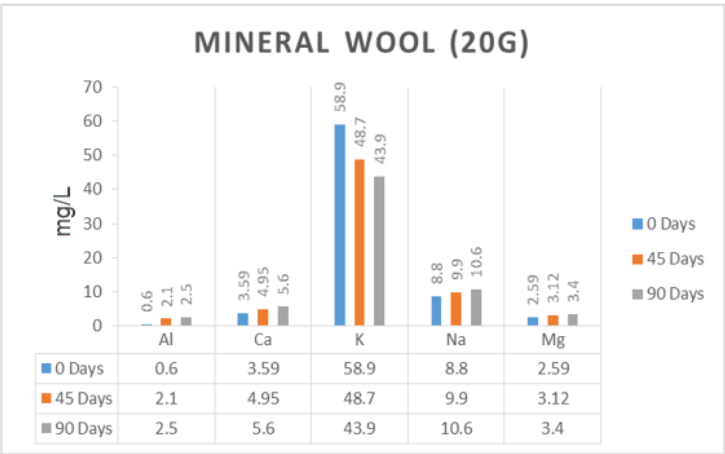

(a)

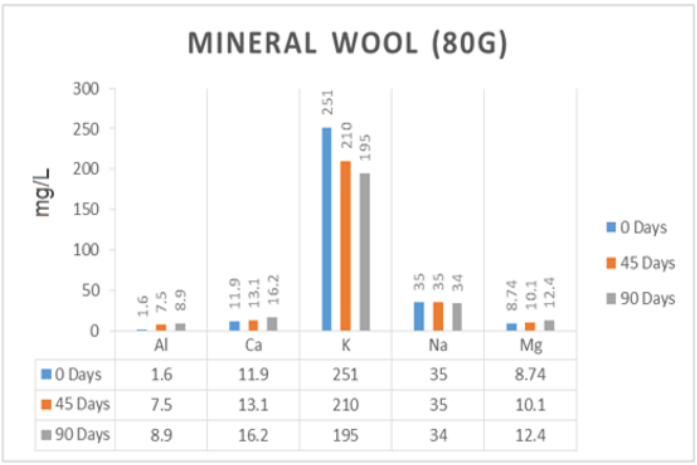

(b)

Figure 35 - ICP analysis was conducted to determine the concentrations (in mg/L) of alkali elements + Al in mineral wool leachate solutions obtained from insulation samples that were aged at 150°C in a furnace for 0-, 45-, and 90-days a) 20g, b) 80g

As can be seen from Figure 35, a subtle rise in alkaline ions (Mg^{2+}, Ca^{2+}, Na^{+} and K^{+}) and Al^{3+} was observed with an increase in the aging process of the insulation. This is due to the likelihood of increased ion release due to the decomposition of organic binders when the insulation is subjected to heat. Cao et al. conducted a study on mild steel corrosion under insulation and the impact of dissolved metal ions. Their findings indicated the presence of four significant cations leached from the mineral wool insulation: Fe^{3+}, Mg^{2+}, Ca^{2+}, and K^{+}. Additionally, a small amount of aluminum (Al) was detected, which can accelerate the corrosion under insulation [29].

4.2.2 Titration tests

The pH of the leachate solutions from mineral wool decreased with both an increasing insulation aging time and an increasing concentration of insulation in solution, as seen in Figure 36. This is due to the fact that when mineral wool insulation ages, it experiences degradation and breakdown, leading to the release of acidic components or compounds into the solution.

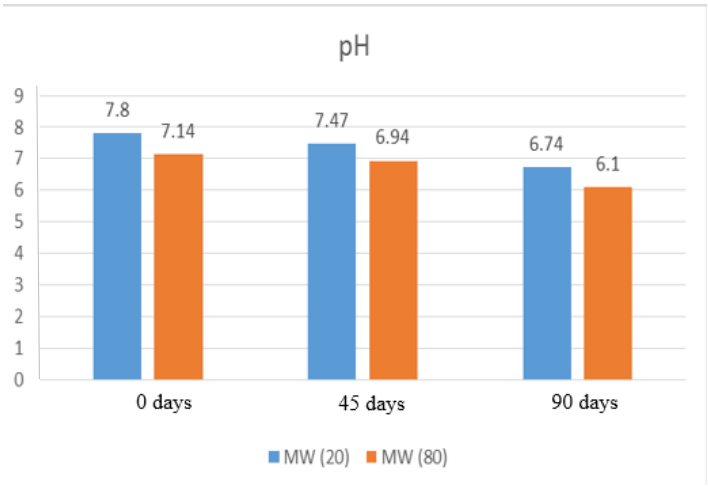

Figure 36 - pH of 20g and 80g mineral wool leachate solutions obtained from insulation samples that were aged at 150°C in a furnace for 0-, 45-, and 90-days

Yang, Liu et al found that a solution in contact with mineral wool insulation will exhibit heightened concentrations of chloride and sulfates ions originating from the insulating materials. These ions have the potential to form strong acids and decrease the pH of the leachate solution [68].

In addition, Tan et al found that an increase in the decomposition of organic matter can affect the pH of the solutions. This is because CO_2 absorbed from the surrounding environment can react with H_2O according to reaction 3, giving rise to carbonic acid (H_2CO_3). The accumulation of H_2CO_3 leads to a reduction in the pH value of the solution [69], [70].

$CO_2 + H_2O \longrightarrow H_2CO_3$ (Reaction 3)

Titration tests were performed on two separate occasions to ensure accuracy, and the resultant average value is meticulously displayed in Table 16 accompanied by the corresponding percentage error.

Table 16 - The mean concentration of HCO_3^- ions in perlite leachate solutions determined through titration, along with the corresponding errors

Solution	**0 - 20**		**0 – 80**		**45 - 20**		**45 - 80**		**90 - 20**		**90 - 80**	
	mg/L	Err	mg/L	Err	mg/L	Err	mg/L	Err	mg/L	Err	mg/L	Err
HCO_3^-	36.6	3%	54.9	3.5%	57.34	2%	73.2	2.5%	61	2.9%	76.86	3%

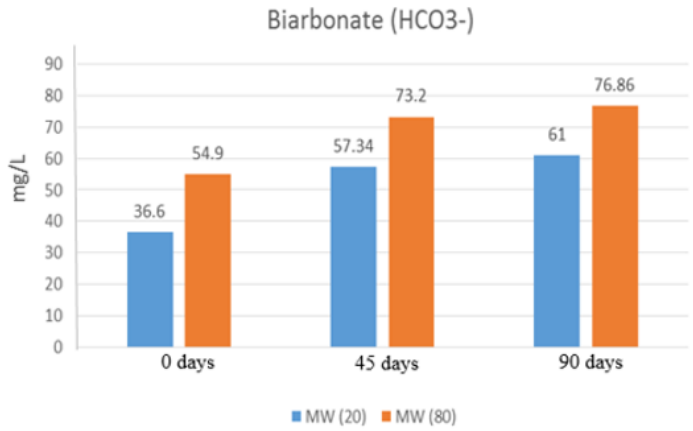

Figure 37 - Concentration of bicarbonate ions (HCO_3^-) in (mg/L) in 20g & 80g mineral wool leachate solutions obtained from insulation samples that were aged at 150°C in a furnace for 0-, 45-, and 90-days

In the chart provided in Figure 37, a clear trend can be observed wherein the concentration of HCO_3^- increases proportionally with both the insulation weight and the duration of the aging process. This is due to the enhanced CO_2 absorption capabilities of the insulation with increasing aging time.

When the generated H_2CO_3 mixes with H_2O it forms HCO_3^- ions according to reaction 4.

$H_2CO_3 + H_2O \longrightarrow HCO_3^- + H_3O^+$ (Reaction 4)

Moreover, when the concentration of HCO_3^- ions increases so does concentration of H^+ increases also, hence the pH value decreases [71].

As per the calculation conducted following ASTM D3875 and referencing Table 5 provided earlier, the presence of CO_3^{2-} and OH^- ions is negligible, registering at a concentration of 0.

4.2.3 Quantitative accelerated laboratory evaluation of leached solutions

4.2.3.1 Mass Loss Corrosion Rate

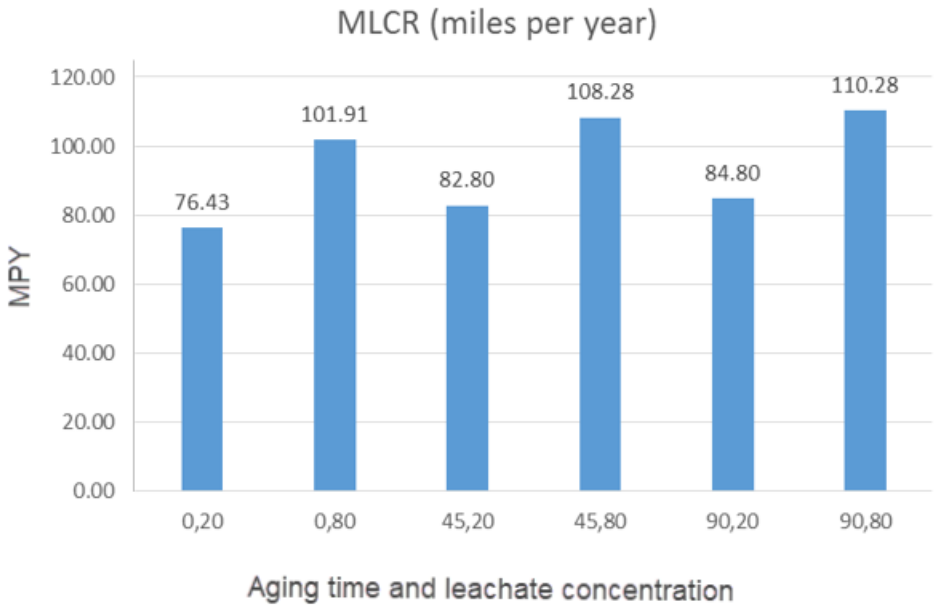

Figure 38 - Mass Loss Corrosion Rate (MLCR) for mineral wool leachate solutions

Figure 38 shows the MLCR of the AISI 1018 samples tested with mineral wool leachate solutions according to the standard ASTM C1617 guidelines. It was evident that the rate increased with an increase in the weight % of the mineral wool insulation and the aging time. This is due to the low pH of the leachate solutions as well as their low resistivity, which allow for fast corrosion kinetics of the steel. This agrees with studies done by Cao et al on mineral wool insulation, where they found that older insulation contains alkaline

oxides and alkaline earth oxides (such as Na_2O, K_2O, CaO, MgO), synthetic resin binders, and refined mineral oil. The dissolved ions leached from this insulation could enhance the electrolyte conductivity and decrease the pH, thus accelerating the kinetics of corrosion and increasing the MLCR [29].

4.2.3.2 Confocal laser microscopy

To further evaluate the influence of the previously mentioned leachate solutions on the steel samples tested according to ASTM 1617 guidelines, surface characterization using confocal laser microscopy was utilized. The blue regions are areas that underwent corrosion.

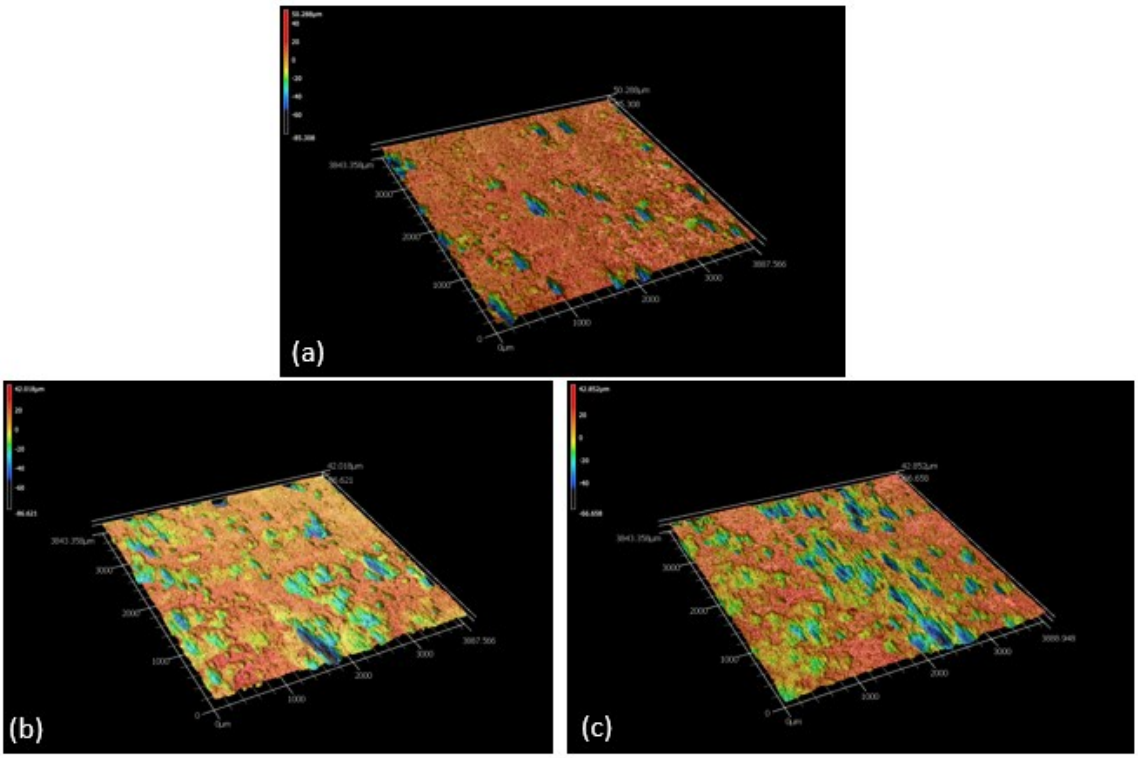

Figure 39 - Confocal laser microscope images of (4 mm x 4 mm scan area) surface of AISI 1018 steel exposed to 20g mineral wool leachate solutions obtained from insulation samples that were aged at 150°C in a furnace for a) 0-, b) 45-, and c) 90-days

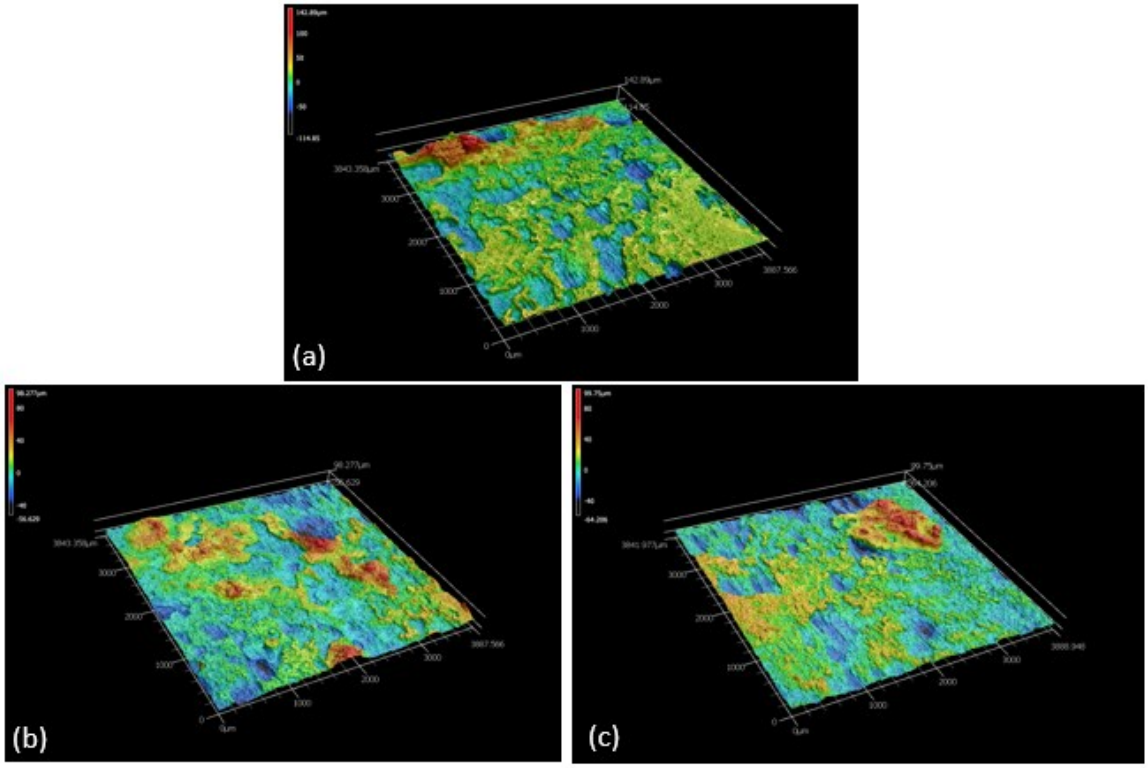

Figure 40 - Confocal laser microscope images of (4 mm x 4 mm scan area) surface of AISI 1018 steel exposed to 80g mineral wool leachate solutions obtained from insulation samples that were aged at 150°C in a furnace for a) 0-, b) 45-, and c) 90-days

Figure 39 & Figure 40 displayed the results obtained from the confocal microscope investigation of AISI 1018 steel samples that were exposed for 4 days to the 20g and 80g mineral wool leachate solutions, prepared from 0, 45 and 90-days aged insulations.

As can be seen from Figure 39 a-c, a gradual reduction in the top layer of the steel's surface is observed (depicted by the orange color), indicating the occurrence of a surface corrosion, which is uniform. Moreover, Figure 39-c exhibits a notable increase in the blue regions, indicating an increase in the degree of uniform corrosion experienced by the steel exposed to the leachate solutions prepared from insulation aged for 90 days. This is due to the decrease in both the pH and the resistivity of the solution, with increasing insulation aging period. Moreover, steels exposed to low pH solutions are subjected to mostly uniform corrosion that increases with a decrease in the solution resistance.

In Figure 40, a more extensive corrosion is apparent, with the dominant presence of the blue color. When compared to the 20g solutions (Figure 40), it becomes evident that as the weight% of mineral wool increases, the corrosion mechanism becomes more pronounced.

This trend remains the same with increasing the duration of the insulation aging process time. This is again due to the low pH and low resistivity of the solution.

4.2.4 High temperature electrochemical testing

4.2.4.1 Potentiodynamic polarization tests

The assessment of corrosion resistance of the autoclave steel samples was carried out quantitatively using linear sweep polarization tests and the resulting data were plotted using potentiodynamic curves, shown in Figure 41 and Figure 42. Electrochemical parameters such as E_{corr}, I_{corr}, CR, and R_p, were extracted using Tafel Extrapolation and are presented in Tables 17-22.

Mineral wool 20 g:

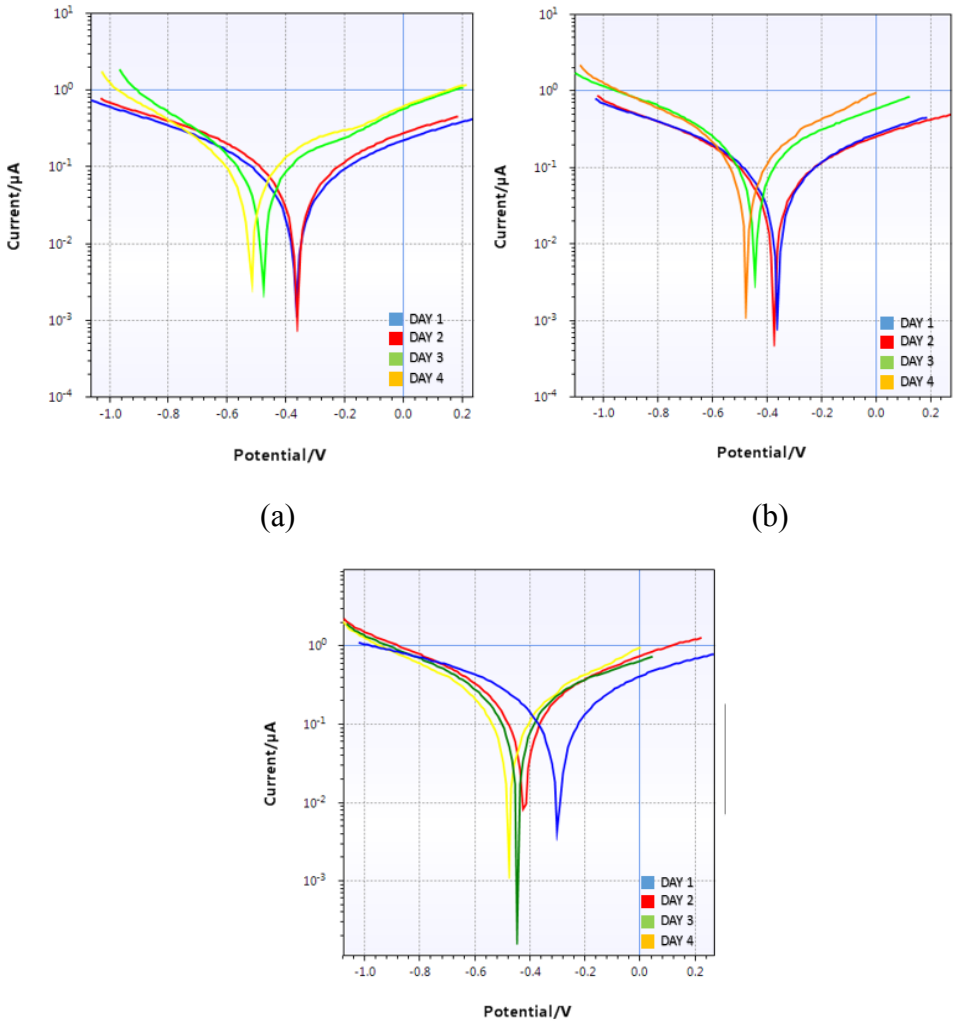

Figure 41 - Potentiodynamic polarization curves were obtained for the API X52 steel electrodes immersed in 20g mineral wool leachate solutions obtained from insulation samples that were aged at 150°C in a furnace for a) 0-, b) 45-, and c) 90-days

Table 17 - Corrosion parameters extracted from potentiodynamic polarization curves measured over 4 days for API X52 electrodes immersed in mineral wool, 0 days, 20g leachate solution.

MW - 0 days - 20g	E_{corr} (V)	I_{corr} (µA)	R_p (KΩ)	CR (mm/year)
Day 1	-0.363	0.106	1.68	0.62
Day 2	-0.362	0.129	1.34	0.75
Day 3	-0.477	0.153	0.92	0.89
Day 4	-0.516	0.182	0.89	1.06

Table 18 - Corrosion parameters extracted from potentiodynamic polarization curves measured over 4 days for API X52 electrodes immersed in mineral wool, 45 days, 20g leachate solution.

MW - 45 days - 20g	E_{corr} (V)	I_{corr} (µA)	R_p (KΩ)	CR (mm/year)
Day 1	-0.362	0.129	1.35	0.75
Day 2	-0.374	0.12	1.40	0.70
Day 3	-0.446	0.243	0.69	1.41
Day 4	-0.477	0.245	0.65	1.42

Table 19 - Corrosion parameters extracted from potentiodynamic polarization curves measured over 4 days for API X52 electrodes immersed in mineral wool, 90 days, 20g leachate solution

MW - 90 days - 20g	E_{corr} (V)	I_{corr} (µA)	R_p (KΩ)	CR (mm/year)
Day 1	-0.331	0.131	0.98	0.76
Day 2	-0.426	0.196	0.93	1.14
Day 3	-0.446	0.249	0.53	1.45
Day 4	-0.477	0.281	0.47	1.63

From Table 17, 14 & 15, it can be seen that the value of E_{corr} decreases with increasing insulation aging time, indicating that the steel surface is becoming more reactive. Thus, the steel samples' resistivity to corrosion decreases. Moreover, this can also be

corroborated by the gradual increase in I_{corr} and CR during the tests, indicating an increase in the corrosion kinetics of the steel samples due to the decreased resistivity of the solution. This behavior is further reinforced by the decrease in the R_p values indicating a decrease in the corrosion resistivity of the steel samples. This is due to the decrease in the pH values of the leachate solutions with increasing insulation aging time. Therefore, in the presence of acidic solutions, the concentration of hydrogen ions (H^+) is notably high. When exposed to an aqueous solution, carbon steel naturally develops a protective layer of iron oxide (Fe_2O_3) on its surface, offering some resistance against corrosion. Nevertheless, in an acidic environment, this protective oxide layer can dissolve readily due to the increased concentration of H^+ ions that react with the metal surface. Consequently, H^+ ions can permeate the carbon steel's protective oxide layer and initiate corrosion processes. This results in an accelerated corrosion rate and compromises the metal's integrity more rapidly. Therefore, the corrosion rate of X52 metal generally increases with decreasing pH values [63].

Mineral wool 80 g:

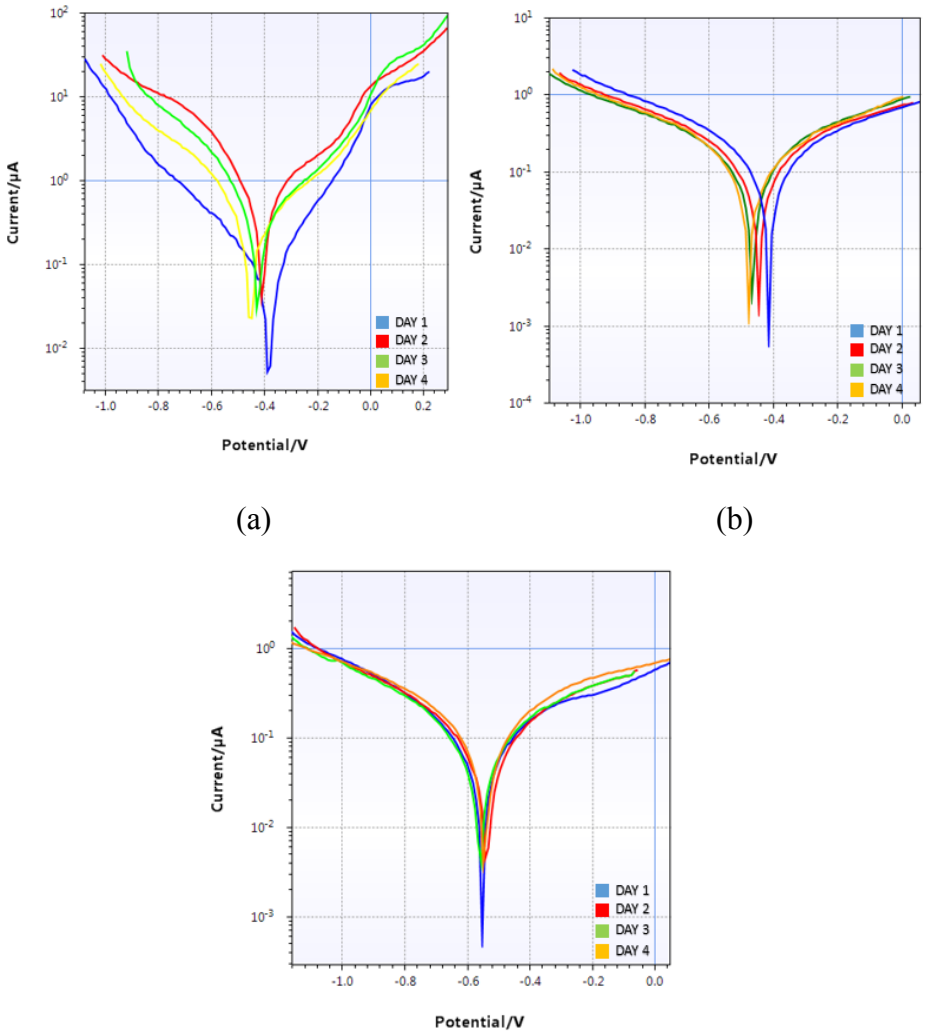

Figure 42 - Potentiodynamic polarization curves were obtained for the API X52 steel electrodes immersed in 80g mineral wool leachate solutions obtained from insulation samples that were aged at 150°C in a furnace for a) 0-, b) 45-, and c) 90-days

Table 20 - Corrosion parameters extracted from potentiodynamic polarization curves measured over 4 days for API X52 electrodes immersed in mineral wool, 0 days, 80 g leachate solution.

MW - 0 days - 80g	E_{corr} (V)	I_{corr} (µA)	R_p (KΩ)	CR (mm/year)
Day 1	-0.388	0.264	0.63	1.53
Day 2	-0.411	0.253	0.64	1.47
Day 3	-0.449	0.245	0.65	1.42
Day 4	-0.429	0.281	0.59	1.63

Table 21 - Corrosion parameters extracted from potentiodynamic polarization curves measured over 4 days for API X52 electrodes immersed in mineral wool, 45 days, 80g leachate solution.

MW - 45 days - 80g	E_{corr} (V)	I_{corr} (µA)	R_p (KΩ)	CR (mm/year)
Day 1	-0.414	0.27	0.81	1.57
Day 2	-0.447	0.264	0.50	1.53
Day 3	-0.466	0.269	0.32	1.56
Day 4	-0.477	0.294	0.27	1.71

Table 22 - Corrosion parameters extracted from potentiodynamic polarization curves measured over 4 days for API X52 electrodes immersed in mineral wool, 90 days, 80g leachate solution.

MW - 90 days - 80g	E_{corr} (V)	I_{corr} (µA)	R_p (KΩ)	CR (mm/year)
Day 1	-0.553	0.28	0.58	1.63
Day 2	-0.544	0.295	0.65	1.71
Day 3	-0.556	0.31	0.59	1.80
Day 4	-0.548	0.33	0.72	1.92

In Table 20, 21 & 22, the E_{corr} value exhibits a decreasing trend both over the duration of the test and with increasing insulation aging time. This decrease indicates the growing susceptibility of the steel samples to corrosion. This is corroborated by the increasing values of I_{corr} and CR and the decreasing values of R_p indicating that the steel samples are corroding actively and that their dissolution rate is increasing with the duration of the test and the aging time of the insulation.

The electrochemical parameters values for the steel samples exposed to the 80 g displayed a similar trend as for those exposed to the 20 g solutions, albeit to a greater extent in the latter solution. This is due to the increase in the acidity of the 80 g solution coupled with the elevated concentration of HCO_3^- renders these solutions particularly conductive to the corrosion process.

4.2.5 Surface characterization

Surface corrosion on autoclave steel samples was investigated utilizing confocal laser microscopy. The results are shown in Figure 43 & Figure 44, where regions appearing in blue highlight sunken or corroded areas. Conversely, areas depicted in dark orange signify untouched or non-corroded regions. The intensity of the blue areas corresponds to the magnitude of corrosion, with deeper shades indicating more pronounced levels of corrosion.

4.2.5.1 Confocal laser microscopy

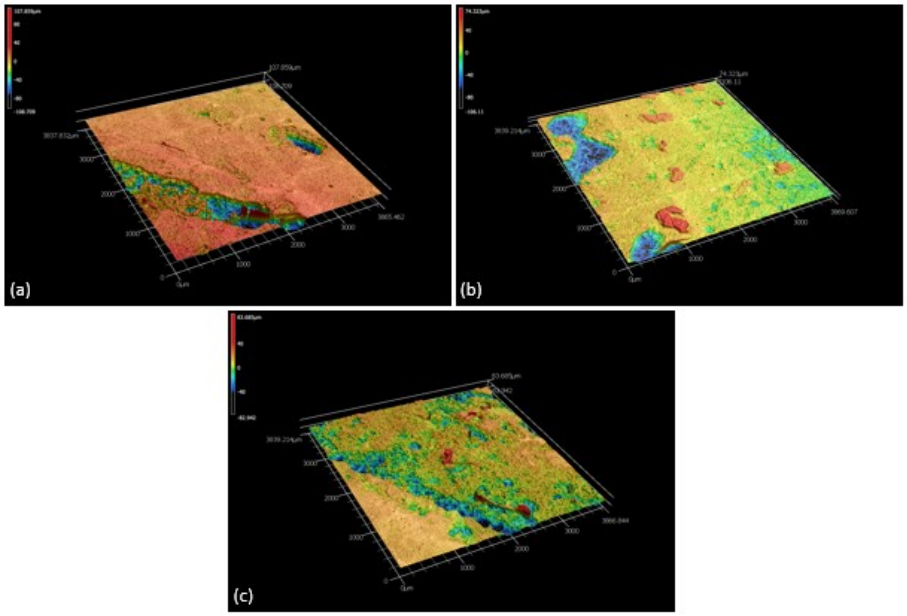

Figure 43 - Confocal laser microscope images of (4 mm x 4 mm scan area) surface of API 5L grade X52 steel tested for 4 days in the autoclave containing 20g mineral wool leachate solutions obtained from insulation samples that were aged at 150°C in a furnace for a) 0- , b) 45-, and c) 90-days

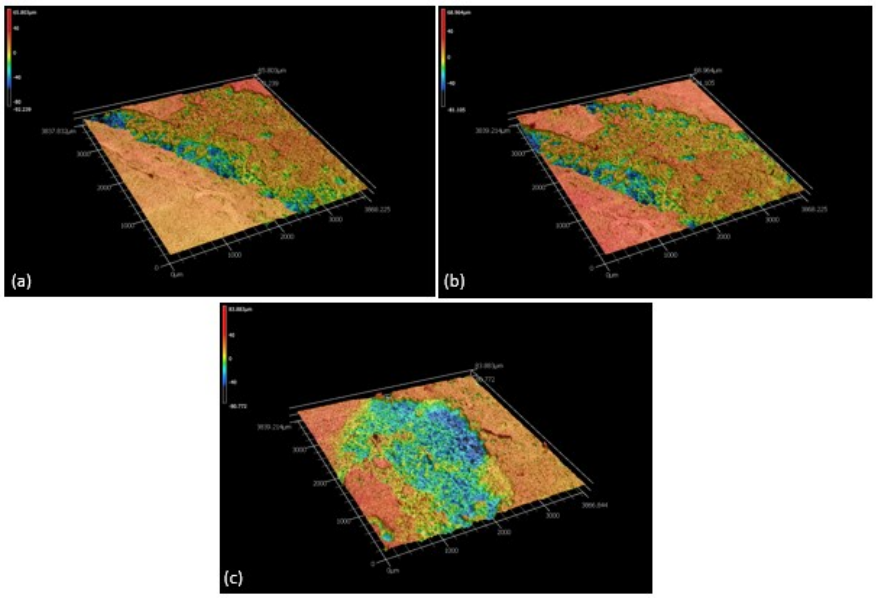

Figure 44 - Confocal laser microscope images of (4 mm x 4 mm scan area) surface of API 5L grade X52 steel tested for 4 days in the autoclave containing 80g mineral wool leachate solutions obtained from insulation samples that were aged at 150°C in a furnace for a) 0- , b) 45-, and c) 90-days

Figure 43-a shows a limited corroded area. However, the significance of corrosion becomes pronounced as solution concentration and aging duration are increased. Notably, in the case of the 80 g solutions, the distinct presence of expansive blue regions vividly underscores the intensified nature of corrosion, indicative of deeper corrosive effects.

As the acidity of a solution increases (Figure 36), the likelihood of corrosion also tends to rise. Acidic solutions can increase the rate of electrochemical reactions, including those involved in corrosion, due to their low resistivity and ionic activities. This acceleration can lead to a more rapid degradation of the metal. Moreover, the presence of hydrogen ions (H^+) in acidic solutions can contribute to the breakdown of protective passivation layers on the metal's surface, making it more susceptible to corrosion. Finally, acidic conditions can promote the formation of corrosive species, such as chloride ions, which can be particularly aggressive in corroding metals. Consequently, the corrosive attack penetrates deeper into the metal surfaces, causing greater material loss and affecting the structural integrity of the samples. The correlation between the concentration of the mineral wool solution and the extent of corrosion highlights the critical role of the solution's chemical composition in driving the degradation of the metal samples [75] ,[74].

4.2.5.2 SEM & EDS

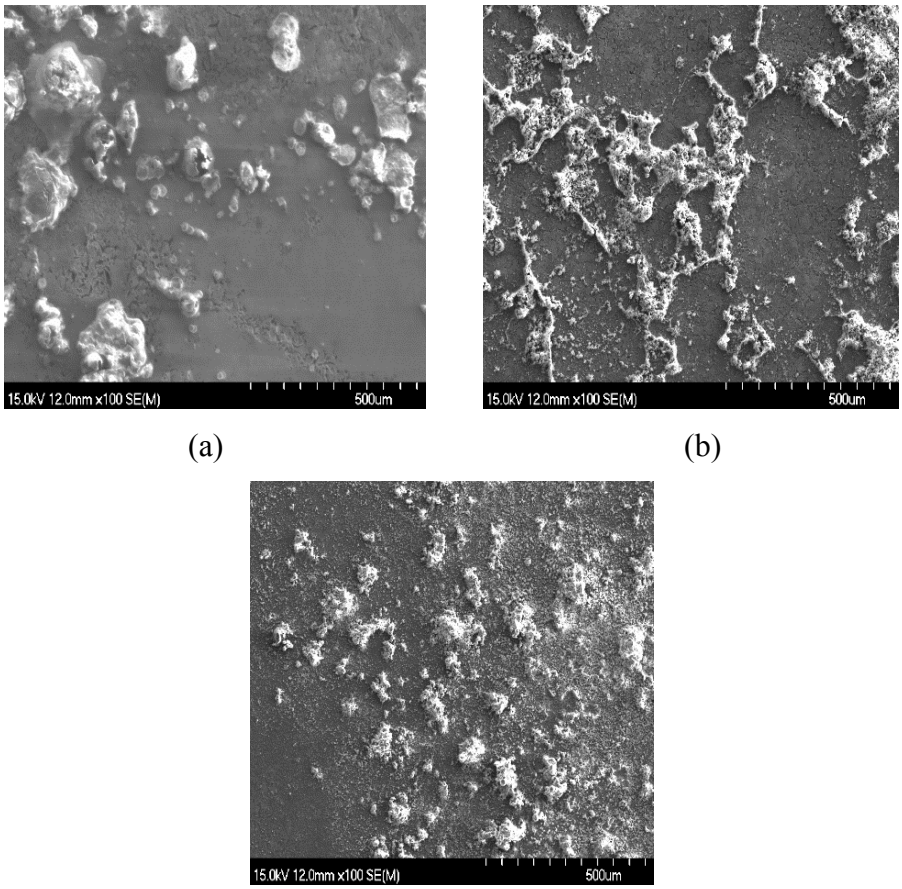

(a) (b)

(c)

Figure 45 - Scanning electron microscope (SEM) micrographs of the surface of X52 steel tested in the autoclave containing 20g mineral wool leachate solutions obtained from insulation samples that were aged at 150°C in a furnace for a) 0-, b) 45-, and c) 90-days

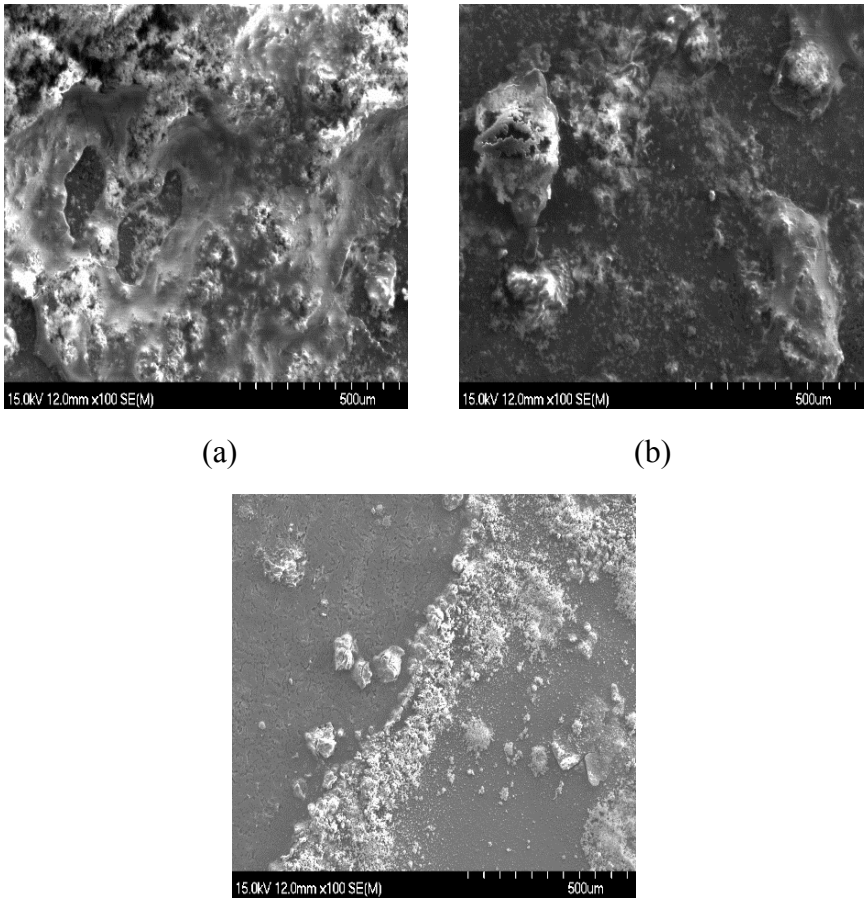

Figure 46 - Scanning electron microscope (SEM) micrographs of the surface of X52 steel tested in the autoclave containing 80g mineral wool leachate solutions obtained from insulation samples that were aged at 150°C in a furnace for a) 0-, b) 45-, and c) 90-days

Upon close examination using Scanning Electron Microscopy (SEM), it becomes evident that the surface of the metal immersed in mineral wool leachate solution exhibits a secondary layer composed of corrosion products. This secondary layer appears to have formed as a result of the intricate chemical reactions taking place between the metal and the mineral-rich leachate solution. The layer is characterized by a distinct texture and composition, differing from the original metal surface. Understanding the formation and characteristics of this secondary layer is crucial in comprehending the metal's long-term behavior and devising effective corrosion protection strategies. Analyzing it using EDS is essential for gaining deeper insights into its chemical composition.

Table 23 - The results of the Energy Dispersive Spectroscopy (EDS) analysis on the corrosion products of the API X52 steel sample immersed in a mineral wool leachate solutions

Elements (% weight)	C	O	Al	Si	Mn	Fe	Total
MW – 0 - 20	9.08	20.13	0.12	0.24	0.88	69.54	100
MW – 45 - 20	7.72	22.8	0.92	0.3	0.71	67.54	100
MW – 90 - 20	7.33	25.66	0.23	0.32	1.02	65.43	100
MW – 0 - 80	5.99	28.78	0.34	0.46	1.14	63.3	100
MW – 45 - 80	4.4	34.43	1.12	0.48	1.18	58.38	100
MW – 90 - 80	4.17	35.54	1.1	0.46	1.13	57.61	100

In the table presented above, a noteworthy observation is the direct correlation between the weight % of oxygen in the corrosion product and the concentration of the solution. As the solution concentration increased, so did the percentage of oxygen in the corrosion product. This finding carries significant implications for our understanding of the corrosion process and its dynamics.

Understanding the percentage of oxygen in the layer that formed on the surface of steel samples immersed in mineral wool leachate solution is of utmost importance. Oxygen plays a critical role in initiating and propagating corrosion reactions in metals, it is directly related to the oxidation state of the iron present in the samples. Higher oxygen levels can accelerate the rate of metal dissolution. Iron can exist in different oxidation states (Figure 2), such as ferrous (Fe^{2+}) and ferric (Fe^{3+}) leading to the formation of various iron oxide species such as Fe_2O_3 (hematite) and Fe_3O_4 (magnetite), depending on the availability of oxygen and the pH of the leachate solution [76], [77].

On the other hand, as the steel corrodes, it loses iron atoms in the form of these corrosion products, which tend to have a lower carbon content than the original steel. The reduction in carbon content occurs because carbon in the steel does not directly participate in the corrosion reaction, while the iron is oxidized and converted into corrosion products. This results in a relatively lower percentage of carbon in the corroded sample compared to the original steel.

Chapter 5: Conclusions

In summary, the comparison between perlite and mineral wool insulation materials in terms of their impact on corrosion reveals intriguing insights into the protective properties of these materials within industrial and commercial settings. This investigation aimed to discern the corrosion patterns exhibited under these two insulation types and shed light on the underlying factors that contribute to such contrasting outcomes. The results underscore the critical importance of insulation selection, not only for its primary thermal and mechanical functions but also for its secondary influence on corrosion mitigation.

- Perlite and mineral wool stand as two prominent contenders in the realm of insulation materials, each possessing distinct characteristics that appeal to various applications. Perlite, a volcanic glass that expands when heated, offers remarkable thermal insulation capabilities along with inherent corrosion-resistant properties. Mineral wool, derived from natural or synthetic minerals, is recognized for its fire resistance and acoustic insulation attributes, yet its interaction with metal substrates has raised concerns about potential corrosion initiation and progression.
- Upon evaluating the corrosion performance of these materials, it became evident that perlite insulation acted as an effective barrier against corrosion, primarily due to the formation of a protective film on metal surfaces. The formation of this protective film arises from the intricate chemical composition of perlite, boasting an abundance of $CO_3^{2-}$and OH^- ions. This composition engenders a profound interaction with metal oxides. Complementing this chemistry, the solutions' notable alkalinity, with pH levels spanning from 10.5 to 11.5 (variations contingent on solution concentration and insulation aging), contributes significantly to the film's genesis. Consequently, the metal remained shielded from moisture, oxygen, and other corrosive elements, preserving its integrity over time.
- This phenomenon was especially pronounced in aggressive environments, such as high-humidity or chemically corrosive settings.
- Conversely, the corrosion observed under mineral wool insulation signaled a more complex interaction between the insulation material, the metal substrate, and the surrounding environment. Mineral wool, while delivering admirable insulation

benefits, appeared to lack the inherent corrosion-resistant properties of perlite. The fibrous nature of mineral wool can trap moisture and corrosive agents, creating microenvironments that promote corrosion initiation, even in situations where the outer conditions might not be overtly corrosive. Furthermore, the deficiency of a protective film analogous to that of perlite significantly compromised the insulation material's capacity to impede the infiltration of corrosive agents. This shortfall can be attributed to the prevalent presence of HCO_3^- ions within the solutions. Additionally, the inherent acidity of these solutions, characterized by a pH spectrum ranging from 6.1 to 7.8, played a crucial role in exacerbating this limitation, allowing them to interact directly with the metal surface. This direct exposure led to localized corrosion, and over time, manifested as visible degradation of the metal.

- It is worth noting that the corrosion tendencies exhibited under mineral wool insulation can be influenced by several variables, including the type of metal substrate, the specific environment, and the installation techniques employed. While mineral wool itself might not possess the corrosion-resistant qualities of perlite.
- The corrosion disparities witnessed under perlite and mineral wool insulation highlight the multifaceted interplay between material properties, environmental factors, and their consequences on metal integrity. Perlite's innate ability to foster a protective film offers a valuable advantage, rendering it a reliable choice for insulation where corrosion control is of paramount concern. On the other hand, mineral wool's corrosion-promoting attributes emphasize the necessity for a comprehensive approach to insulation selection and system design.

In conclusion, as industries continue to explore innovative solutions for enhanced energy efficiency, the findings of this study urge engineers, designers, and facility managers to meticulously evaluate insulation materials based not only on their thermal performance but also on their potential influence on corrosion. The development of new insulation formulations that combine the positive attributes of materials like perlite and mineral wool while addressing their shortcomings could potentially lead to novel corrosion-resistant insulation options. Moreover, the insights gleaned from this investigation contribute to the

broader understanding of corrosion mechanisms, ultimately steering the industrial community toward more informed choices in insulation strategies and materials.

References

[1] Z. Ahmad, *Principles of corrosion engineering and corrosion control*, 1st ed. Amsterdam ; Boston, Mass: Elsevier/BH, 2006.

[2] "Anodes, Zinc, Magnesium, Aluminum and Galvanic Corrosion on Boats." http://www.pcmarinesurveys.com/Anodes,%20Zincs,%20Aluminum,%20Magnesium%20and%20Boat%20Corrosion.htm (accessed Aug. 26, 2023).

[3] B. Beverskog and I. Puigdomenech, "Revised pourbaix diagrams for iron at 25–300 °C," *Corrosion Science*, vol. 38, no. 12, pp. 2121–2135, Dec. 1996, doi: 10.1016/S0010-938X(96)00067-4.

[4] P. P. Milella, *Fatigue and Corrosion in Metals*. Milano: Springer Milan, 2013. doi: 10.1007/978-88-470-2336-9.

[5] "Uniform Corrosion - AMPP." https://www.ampp.org/technical-research/impact/corrosion-basics/group-1/uniform-corrosion (accessed Aug. 23, 2023).

[6] P. R. Roberge, *Corrosion engineering: principles and practice*. New York: McGraw-Hill, 2008.

[7] E. P. Grishina and A. V. Noskov, *Electrochemical oxidation and corrosion of metals*. New York: Nova Science Publishers, 2010.

[8] "What is crevice corrosion? What are its effects on pipelines?," *Quora*. https://www.quora.com/What-is-crevice-corrosion-What-are-its-effects-on-pipelines (accessed Aug. 23, 2023).

[9] "9 Different Types of Corrosion," *The Constructor*, Aug. 13, 2019. https://theconstructor.org/structural-engg/steel/different-types-corrosion/35536/ (accessed Aug. 23, 2023).

[10] "Different Types of Corrosion: Hydrogen Blistering -Causes and Prevention. WebCorr Corrosion Consulting Services, Corrosion Short Courses and Corrosion Expert Witness. corrosion types, corrosion forms, pipe corrosion, generalized corrosion, pitting corrosion, galvanic corrosion, MIC corrosion, erosion corrosion, corrosion under insulation, M.I.C., MIC, CUI corrosion." https://www.corrosionclinic.com/types_of_corrosion/hydrogen-blistering-HB.htm (accessed Aug. 26, 2023).

[11] Q. Cao *et al.*, "A Review of Corrosion under Insulation: A Critical Issue in the Oil and Gas Industry," *Metals*, vol. 12, no. 4, p. 561, Mar. 2022, doi: 10.3390/met12040561.

[12] I. M. Funderburg, “An Industry Perspective:Revisiting Recommendations,” Insulation Outlook Magazine, 2006.

[13] K. A. Chandler, *Marine and offshore corrosion*. in Marine engineering series. London ; Boston: Butterworths, 1985.

[14] F. Flow, “#EpicFail: Corrosion Under Insulation,” *R-TECH Materials*, Oct. 31, 2022. https://www.r-techmaterials.com/news-and-blog/epicfail-corrosion-under-insulation/ (accessed Aug. 23, 2023).

[15] R. Norsworthy and P. J. Dunn, “Control of corrosion under insulation,” ASHRAE Journal, 2003.

[16] R. Javaherdasht, “Corrosion under Insulation (CUI): A review of essential knowledge and practice,” *JMSSE*, vol. Vol. 1 (2), 2014, p. pp 36-43, Jun. 2014.

[17] E. O. Eltai, F. Musharavati, and E. Mahdi, “Severity of corrosion under insulation (CUI) to structures and strategies to detect it,” *Corrosion Reviews*, vol. 37, no. 6, pp. 553–564, Nov. 2019, doi: 10.1515/corrrev-2018-0102.

[18] H. S. Ahluwalia, “An In-Depth Analysis,” Insulation Outlook Magazine, 2006.

[19] P. P. Langroudi and I. Weidlich, “Applicable Predictive Maintenance Diagnosis Methods in Service-Life Prediction of District Heating Pipes,” *Environmental and Climate Technologies*, vol. 24, no. 3, pp. 294–304, Nov. 2020, doi: 10.2478/rtuect-2020-0104.

[20] J. F. Delahunt, “Corrosion Under Thermal Insulation and Fireproofing - An Overview,” 2003.

[21] K. Posteraro, “Thwart corrosion under industrial insulation,” *American Institute of Chemical Engineers*, vol. 95, no. 10, p. 43, Oct. 1999.

[22] O. Hill, *How Dry is your Insulation*. IOM Corrosion Under Insulation Conference, Sheffield, United Kingdom, 2004.

[23] P. E. Schweitzer Philip A., *Fundamentals of Metallic Corrosion: Atmospheric and Media Corrosion of Metals*, 0 ed. CRC Press, 2006. doi: 10.1201/9780849382444.

[24] A. Marquez, J. Singh, and C. Maharaj, “Corrosion Under Insulation Examination to Prevent Failures in Equipment at a Petrochemical Plant,” *J Fail. Anal. and Preven.*, vol. 21, no. 3, pp. 723–732, Jun. 2021, doi: 10.1007/s11668-021-01135-5.

[25] Leidheiser Henry Jr, “Corrosion Control under Thermal Insulation and Fireproofing,” *NACE International*.

[26] M. J. Lettich, “Is There a Cure for CorrosionUnder Insulation?,” 2005.

[27] C. T. Petry, D. T. Costa, and A. Droste, “Removal of ammoniacal nitrogen from municipal landfill leachate with floating *Typha domingensis* (Typhaceae),” *Acta biol. Colomb.*, vol. 25, no. 1, pp. 5–13, Jan. 2020, doi: 10.15446/abc.v25n1.74749.

[28] W. Rykała, M. J. Fabiańska, and D. Dąbrowska, “The Influence of a Fire at an Illegal Landfill in Southern Poland on the Formation of Toxic Compounds and Their Impact on the Natural Environment,” *IJERPH*, vol. 19, no. 20, p. 13613, Oct. 2022, doi: 10.3390/ijerph192013613.

[29] Q. Cao, M. Esmaily, R. L. Liu, N. Birbilis, and S. Thomas, “Corrosion of mild steel under insulation – the effect of dissolved metal ions,” *Corrosion Engineering, Science and Technology*, vol. 55, no. 4, pp. 322–330, May 2020, doi: 10.1080/1478422X.2020.1734737.

[30] M. J. Cullin, G. Birmingham, R. Srinivasan, and G. Hailu, “Injectable Sodium Bentonite Inhibitors for Corrosion under Insulation,” *J. Pipeline Syst. Eng. Pract.*, vol. 11, no. 4, p. 04020036, Nov. 2020, doi: 10.1061/(ASCE)PS.1949-1204.0000488.

[31] O. Lavigne, A. Kotousov, and V. Luzin, “Microstructural, Mechanical, Texture and Residual Stress Characterizations of X52 Pipeline Steel,” *Metals*, vol. 7, no. 8, p. 306, Aug. 2017, doi: 10.3390/met7080306.

[32] L. M. Quej-Ake and A. Contreras, “Electrochemical study on the corrosion rate of X52 steel exposed to different soils,” *ACMM*, vol. 65, no. 1, pp. 97–106, Jan. 2018, doi: 10.1108/ACMM-12-2016-1737.

[33] L. D. Maxim, R. Niebo, and E. E. McConnell, “Perlite toxicology and epidemiology – a review,” *Inhalation Toxicology*, vol. 26, no. 5, pp. 259–270, Apr. 2014, doi: 10.3109/08958378.2014.881940.

[34] K. Drozdzol, “Thermal and Mechanical Studies of Perlite Concrete Casing for Chimneys in Residential Buildings,” *Materials*, vol. 14, no. 8, p. 2011, Apr. 2021, doi: 10.3390/ma14082011.

[35] K. D. Timmerhaus, Ed., *Proceedings of the 1962 Cryogenic Engineering Conference: University of California, Los Angeles, California, August 14-16, 1962*. New York: Springer Science+Business Media, 1963.

[36] I. Suherman, A. Wahyudi, H. E. Mamby, and D. A. Darmawan, “Expanded perlite commercialization techno-economic analysis in Indonesia,” *IOP Conf. Ser.: Earth Environ. Sci.*, vol. 882, no. 1, p. 012085, Nov. 2021, doi: 10.1088/1755-1315/882/1/012085.

[37] “Wool Insulation Pros And Cons: The Great Debate,” *Home Logic UK*. http://www.homelogic.co.uk/wool-insulation-pros-and-cons-the-great-debate (accessed May 24, 2023).

[38] "Advantages of mineral wool insulation - Thermal Resource Management." https://thermal-resources.com/advantages-of-mineral-wool-insulation/ (accessed May 24, 2023).

[39] M. Amin, M. Akbar, and M. Salman, "Composite insulators and their aging: An overview," *Sci. China Ser. E-Technol. Sci.*, vol. 50, no. 6, pp. 697–713, Dec. 2007, doi: 10.1007/s11431-007-0053-x.

[40] K. D. Ralston, "Laboratory Testing in Leachate Environments to Understand Stress Corrosion Cracking on an Insulated Above-Ground Pipeline," *NACE International*, vol. 2019–13438, Mar. 2019.

[41] C16 Committee, "Test Methods for Chemical Analysis of Thermal Insulation Materials for Leachable Chloride, Fluoride, Silicate, and Sodium Ions," ASTM International. doi: 10.1520/C0871-18.

[42] Jun, Shinhee, Kim, Jun-Ho, Kim, Sunkwang, You, Yong Zoo, and Cha, Byung-Chul, "Mechanical and Chemical Characterization of NbN_x Coatings Deposited by ICP Assisted DC Magnetron Sputtering," *Journal of the Korean Society for Heat Treatment*, vol. 27, no. 1, pp. 10–14, Jan. 2014, doi: 10.12656/JKSHT.2014.27.1.10.

[43] S. N. Wren and D. J. Donaldson, "How does deposition of gas phase species affect pH at frozen salty interfaces?," *Atmos. Chem. Phys.*, vol. 12, no. 21, pp. 10065–10073, Nov. 2012, doi: 10.5194/acp-12-10065-2012.

[44] D19 Committee, "Test Method for Alkalinity in Brackish Water, Seawater, and Brines," ASTM International. doi: 10.1520/D3875-15R23.

[45] "Understanding ASTM Test Methods Evaluating Thermal Insulations and Corrosion of Metals - Insulation Outlook Magazine." https://insulation.org/io/articles/understanding-astm-test-methods-evaluating-thermal-insulations-and-corrosion-of-metals/ (accessed Jun. 07, 2023).

[46] "Measuring Corrosion Using the ASTM C1617 Test Method." https://www.jm.com/en/blog/2015/march/measuring-corrosion-using-the-astm-c1617-test-method/ (accessed Jun. 08, 2023).

[47] S. H. Tuna, N. O. Pekmez, F. Keyf, and F. Canli, "The electrochemical properties of four dental casting suprastructure alloys coupled with titanium implants," *J. Appl. Oral Sci.*, vol. 17, no. 5, pp. 467–475, Oct. 2009, doi: 10.1590/S1678-77572009000500022.

[48] F. Wang *et al.*, "Corrosion Mechanism of L360 Pipeline Steel Coated with S8 in CO2-Cl− System at Different pH Values," *Metals*, vol. 11, no. 12, p. 1975, Dec. 2021, doi: 10.3390/met11121975.

[49] J. Ye *et al.*, “Experimental investigations on water absorption and mechanical properties of expanded perlite mortar under accelerated and natural aging conditions,” *Mater. Res. Express*, vol. 9, no. 6, p. 065506, Jun. 2022, doi: 10.1088/2053-1591/ac79a7.

[50] F. Wang, X. Xiao, T. Mi, and C. Dong, “Numerical Simulation of the Release of Alkali Metal during the Combustion of Biomass-fired Boiler:,” presented at the 2015 International Conference on Materials, Environmental and Biological Engineering, Guilin, China, 2015. doi: 10.2991/mebe-15.2015.168.

[51] B. Plešingerová and E. Dedinská, “STUDY OF INFLUENCE OF pH VALUE ON REMOVING OF Cu2+ IONS FROM SOLUTION ONTO PERLITE,” *Acta Metall Slovaca*, vol. 20, no. 3, pp. 309–317, Sep. 2014, doi: 10.12776/ams.v20i3.327.

[52] J. Basmal, M. L. Henrida, R. Kusumawati, and N. Nurhayati, “Growth Hormone, Nitrogen and Potassium Content in The Formulated Solid Waste from Agar Processing for Fertilizer Application,” *Squalen Bull. Marine Fisheries Postharvest Biotech.*, vol. 14, no. 3, p. 131, Dec. 2019, doi: 10.15578/squalen.v14i3.385.

[53] G. Yang *et al.*, “A review of microbial corrosion in reclaimed water pipelines: challenges and mitigation strategies,” *Water Practice and Technology*, vol. 17, no. 3, pp. 731–748, Mar. 2022, doi: 10.2166/wpt.2022.007.

[54] J. Saber, “A mechanism for sodium oxide catalyzed CO2 gasification of carbon,” *Journal of Catalysis*, vol. 109, no. 2, pp. 329–346, Feb. 1988, doi: 10.1016/0021-9517(88)90216-3.

[55] Q. Wu, Z. Zhang, Y. Wang, F. Wang, and Y. Ma, “Experimental study on interface characteristics of liquid sodium-water vapor interaction in SWR,” *International Journal of Thermal Sciences*, vol. 186, p. 108139, Apr. 2023, doi: 10.1016/j.ijthermalsci.2022.108139.

[56] M. Criado, B. Walkley, X. Ke, J. Provis, and S. Bernal, “Slag and Activator Chemistry Control the Reaction Kinetics of Sodium Metasilicate-Activated Slag Cements,” *Sustainability*, vol. 10, no. 12, p. 4709, Dec. 2018, doi: 10.3390/su10124709.

[57] J. W. Schultze and M. M. Lohrengel, “Stability, reactivity and breakdown of passive films. Problems of recent and future research,” *Electrochimica Acta*, vol. 45, no. 15–16, pp. 2499–2513, May 2000, doi: 10.1016/S0013-4686(00)00347-9.

[58] “What is a Passive Film? - Definition from Corrosionpedia.” https://www.corrosionpedia.com/definition/1615/passive-film (accessed Jun. 27, 2023).

[59] C.-O. A. Olsson and D. Landolt, “Passive films on stainless steels—chemistry, structure and growth,” *Electrochimica Acta*, vol. 48, no. 9, pp. 1093–1104, Apr. 2003, doi: 10.1016/S0013-4686(02)00841-1.

[60] G. S. Frankel, “Pitting Corrosion of Metals: A Review of the Critical Factors,” *J. Electrochem. Soc.*, vol. 145, no. 6, pp. 2186–2198, Jun. 1998, doi: 10.1149/1.1838615.

[61] C. Y. Chao, L. F. Lin, and D. D. Macdonald, “A Point Defect Model for Anodic Passive Films: I . Film Growth Kinetics,” *J. Electrochem. Soc.*, vol. 128, no. 6, pp. 1187–1194, Jun. 1981, doi: 10.1149/1.2127591.

[62] A. H. M. Yusop, N. M. Daud, H. Nur, M. R. A. Kadir, and H. Hermawan, “Controlling the degradation kinetics of porous iron by poly(lactic-co-glycolic acid) infiltration for use as temporary medical implants,” *Sci Rep*, vol. 5, no. 1, p. 11194, Jun. 2015, doi: 10.1038/srep11194.

[63] F. F. Eliyan, J. R. Kish, and A. Alfantazi, “Voltammetric Analysis on the Formation of Fe(OH)2 and FeCO3, and on the Reactivity of Passivation of Steel in Carbonate Solutions,” *J. of Materi Eng and Perform*, vol. 24, no. 6, pp. 2473–2480, Jun. 2015, doi: 10.1007/s11665-015-1525-y.

[64] I. V. Artamonova, I. G. Gorichev, and E. B. Godunov, “Effect of Carbonate Ions on Steel 10 Corrosion and Electrochemical Behavior,” *Chem Petrol Eng*, vol. 52, no. 9–10, pp. 710–716, Jan. 2017, doi: 10.1007/s10556-017-0257-2.

[65] P. M. Gil, M. Palomar-Pardavé, M. G. Montes De Oca-Yemha, M. T. Ramírez-Silva, C. Ángeles-Chávez, and M. Romero-Romo, “Effect of Carbonate and Chloride Ions on the Corrosion Susceptibility of Pipeline Steel Samples Artificially Aged,” *International Journal of Electrochemical Science*, vol. 13, no. 2, pp. 1844–1858, Feb. 2018, doi: 10.20964/2018.02.53.

[66] Z. Zhu, S. Li, and R. Zhang, “Investigation of corrosion characteristics of Cu-10Ni-1.2Fe- *x* Mn (*x* = 0.53, 0.87, 1.19) alloy in 3.5% NaCl solution,” *RSC Adv.*, vol. 11, no. 19, pp. 11318–11328, 2021, doi: 10.1039/D0RA10678J.

[67] J. W. Park, K. Y. Ann, and C.-G. Cho, “Resistance of Alkali-Activated Slag Concrete to Chloride-Induced Corrosion,” *Advances in Materials Science and Engineering*, vol. 2015, pp. 1–7, 2015, doi: 10.1155/2015/273101.

[68] M. Yang and J. Liu, “In Situ Monitoring of Corrosion under Insulation Using Electrochemical and Mass Loss Measurements,” *International Journal of Corrosion*, vol. 2022, pp. 1–12, Jan. 2022, doi: 10.1155/2022/6681008.

[69] R. Sadono, G. Irya Ichriani, F. Fahrunsyah, Y. Nuraini, and E. Handayanto, “Productivity evaluation of Eucalyptus urophylla plantation established in dryland ecosystems, East Nusa Tenggara,” *J.Degrade.Min.Land Manage.*, vol. 8, no. 1, pp. 2471–2480, Sep. 2020, doi: 10.15243/jdmlm.2020.081.2471.

[70] S. Hussain, D. Bhunia, and S. B. Singh, “An Experimental Investigation of Accelerated Carbonation on Properties of Concrete,” *EJ*, vol. 20, no. 2, pp. 29–38, May 2016, doi: 10.4186/ej.2016.20.2.29.

[71] Tai, Y. T., Najimudin, N., and Sudesh, K., "Characteristics of limestone soil collected from Gunung Lang, Perak and metagenomic analysis of the soil microbial community," *MJM*, Dec. 2015, doi: 10.21161/mjm.73115.

[72] T. Peme, L. Olasunkanmi, I. Bahadur, A. Adekunle, M. Kabanda, and E. Ebenso, "Adsorption and Corrosion Inhibition Studies of Some Selected Dyes as Corrosion Inhibitors for Mild Steel in Acidic Medium: Gravimetric, Electrochemical, Quantum Chemical Studies and Synergistic Effect with Iodide Ions," *Molecules*, vol. 20, no. 9, pp. 16004–16029, Sep. 2015, doi: 10.3390/molecules200916004.

[73] SI «Institute of Environmental Geochemistry of NAS of Ukraine», B. Shabalin, O. Lavrynenko, S. Buhera, and N. Mitsiuk, "PHASE FORMATION PROCESSES IN STEEL – BENTONITE INTERFACE IN THE CONDITIONS OF RADIOACTIVE WASTE GEOLOGICAL REPOSITORY EVOLUTION," *Geohìm. tehnog.*, vol. 29, no. 1, pp. 13–23, 2019, doi: 10.15407/geotech2019.29.013.

[74] K. Ivanov, A. Zhukov, E. Bobrova, E. Zhukova, and K. Wako, "Thermal insulation shaped mineral wool products with effective binder," *E3S Web Conf.*, vol. 110, p. 02024, 2019, doi: 10.1051/e3sconf/201911002024.

[75] O. Aykanat and M. Ermeydan, "Production and Characterization of Polylactic acid/Rock wool Biocomposites," *Journal of Innovative Science and Engineering (JISE)*, vol. 4, no. 1, pp. 1–10, Apr. 2020, doi: 10.38088/jise.691237.

[76] M. Uyama, H. Saito, and T. Iioka, "Heating impact on corrosion mechanism of carbon steel surrounded by bentonite," *Mechanical Engineering Journal*, vol. 8, no. 4, pp. 20-00492-20–00492, 2021, doi: 10.1299/mej.20-00492.

[77] V. Johnsirani, J. Sathiyabama, S. Rajendran, and A. S. Prabha, "Inhibitory Mechanism of Carbon Steel Corrosion in Sea Water by an Aqueous Extract of Henna Leaves," *ISRN Corrosion*, vol. 2012, pp. 1–9, Dec. 2012, doi: 10.5402/2012/574321.